Origin of the Red Shifts in the Optical Absorption Bands of Nonplanar Tetraalkylporphyrins

ARTICLE *in* JOURNAL OF THE AMERICAN CHEMICAL SOCIETY · MARCH 2003

Impact Factor: 12.11 · DOI: 10.1021/ja0280933 · Source: PubMed

6 AUTHORS, INCLUDING:

Craig Medforth
University of Porto
167 PUBLICATIONS **6,016** CITATIONS
SEE PROFILE

John A Shelnutt
University of Georgia
265 PUBLICATIONS **8,789** CITATIONS
SEE PROFILE

J|A|C|S
ARTICLES
Published on Web 01/08/2003

Origin of the Red Shifts in the Optical Absorption Bands of Nonplanar Tetraalkylporphyrins

Raid E. Haddad,[†,‡] Stéphanie Gazeau,[§] Jacques Pécaut,[§] Jean-Claude Marchon,*[,§] Craig J. Medforth,*[,‡] and John A. Shelnutt*[,‡,⊥]

Contribution from the Department of Chemical and Nuclear Engineering, University of New Mexico, Albuquerque, New Mexico 87131, Biomolecular Materials and Interfaces Department, Sandia National Laboratories, Albuquerque, New Mexico 87185-1349, Laboratoire de Chimie Inorganique et Biologique (Unité Mixte de Recherche 5046 du Centre National de la Recherche Scientifique, du Commissariat à l'Energie Atomique, et de l'Université Joseph Fourier), Département de Recherche Fondamentale sur la Matière Condensée, CEA-Grenoble, 38054 Grenoble, France, and Department of Chemistry, University of Georgia, Athens, Georgia 30602-2556

Received August 9, 2002; E-mail: jasheln@unm.edu; jcmarchon@cea.fr; medforth@unm.edu

Abstract: The view that the large red shifts seen in the UV−visible absorption bands of peripherally crowded nonplanar porphyrins are the result of nonplanar deformations of the macrocycle has recently been challenged by the suggestion that the red shifts arise from substituent-induced changes in the macrocycle bond lengths and bond angles, termed in-plane nuclear reorganization (IPNR). We have analyzed the contributions to the UV−visible band shifts in a series of nickel or zinc *meso*-tetraalkylporphyrins to establish the origins of the red shifts in these ruffled porphyrins. Structures were obtained using a molecular mechanics force field optimized for porphyrins, and the nonplanar deformations were quantified by using normal-coordinate structural decomposition (NSD). Transition energies were calculated by the INDO/S semiempirical method. These computational studies demonstrate conclusively that the large Soret band red shifts (~40 nm) seen for very nonplanar *meso*-tetra(*tert*-butyl)porphyrin compared to *meso*-tetra(methyl)porphyrin are primarily the result of nonplanar deformations and not IPNR. Strikingly, nonplanar deformations along the high-frequency $2B_{1u}$ and $3B_{1u}$ normal coordinates of the macrocycle are shown to contribute significantly to the observed red shifts, even though these deformations are an order of magnitude smaller than the observed ruffling ($1B_{1u}$) deformation. Other structural and electronic influences on the UV−visible band shifts are discussed and problems with the recent studies are examined (e.g., the systematic underestimation of the $2B_{1u}$ and $3B_{1u}$ modes in artificially constrained porphyrin structures that leads to a mistaken attribution of the red shift to IPNR). The effect of nonplanar deformations on the UV−visible absorption bands is then probed experimentally with a series of novel bridled nickel chiroporphyrins. In these compounds, the substituent effect is essentially invariant and the amount of nonplanar deformation decreases as the length of the straps connecting adjacent *meso*-cyclopropyl substituents decreases (the opposite of the effect observed for conventional strapped porphyrins). Several spectroscopic markers for nonplanarity (UV−visible bands, resonance Raman lines, and ^{1}H NMR resonances) are found to correlate with time-averaged deformations obtained from an NSD analysis of molecular dynamics snapshot structures. These results suggest that UV−visible band shifts of tetrapyrroles in proteins are potentially useful indicators of changes in nonplanarity provided other structural and electronic factors can be eliminated.

Introduction

Although the porphyrin ring is aromatic, it has been found to be highly flexible, and various ways of inducing nonplanar deformations of the macrocycle are known.[1] One strategy frequently employed is to introduce steric crowding of substituents at the porphyrin periphery, that is, either by substitution with many moderately bulky groups (e.g., porphyrins **1**−**4**) or by adding a few very bulky substituents (e.g., **5**). The overcrowding approach often leads to a ruffle (*ruf*) deformation[2] (see Figure 1), a saddle (*sad*) deformation, a mixture of these two deformations, or occasionally other types of deformation, depending upon the specific substituents.[1] Bulky meso alkyl substituents produce predominantly the *ruf* deformation.[3−5] *Ruf* and *sad* deformations in particular are known to result in

* Corresponding Author: John A Shelnutt, Advanced Materials Laboratory, Sandia National Laboratories, 1001 University Blvd SE, Albuquerque, NM 87106. Phone: 505-272-7160. FAX: 505-272-7077.
† University of New Mexico.
‡ Sandia National Laboratories.
§ Département de Recherche Fondamentale sur la Matière Condensée.
⊥ University of Georgia.

(1) Senge, M. O. In *The Porphyrin Handbook*; Kadish, K. M., Smith, K. M., Guilard, R., Eds.; Academic Press: Boston, 2000; Vol. 1, p 239.
(2) Scheidt, W. R.; Lee, Y. J. *Struct. Bonding (Berlin)* **1987**, *64*, 1.
(3) Veyrat, M.; Maury, O.; Faverjon, F.; Over, D. E.; Ramasseul, R.; Marchon, J.-C.; Turowska-Tyrk, I.; Scheidt, W. R. *Angew. Chem., Int. Ed. Engl.* **1994**, *33*, 220.

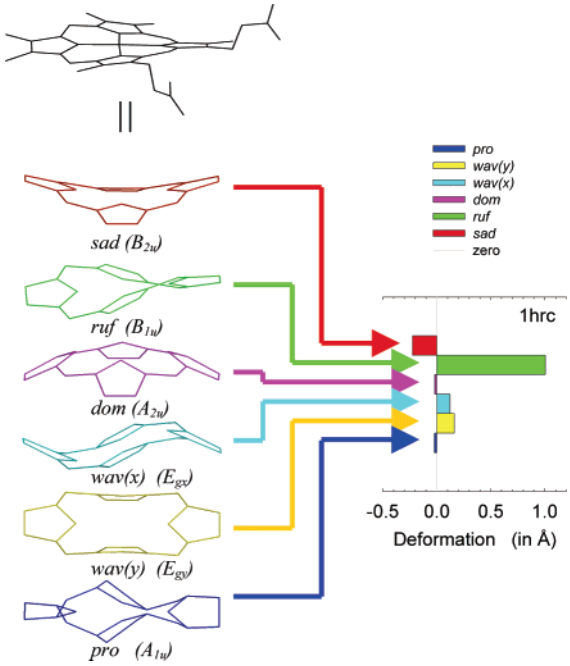

Figure 1. Illustration of the normal-coordinate structural decomposition (NSD) technique, which determines the displacements along all 66 in-plane and out-of-plane normal coordinates that make up a porphyrin structure, illustrated here for only the lowest-frequency out-of-plane modes. A 2-Å deformation is illustrated for each of these normal coordinates. The lowest-frequency out-of-plane deformations of each symmetry type are the primary contributors to the structures of most nonplanar porphyrins.

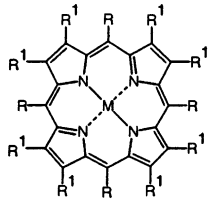

1 R = C_6H_5, R^1 = CH_2CH_3
2 R = R^1 = C_6H_5
3 R = C_6H_5, R^1 = Br
4 R = NO_2, R^1 = CH_2CH_3
5 R = $C(CH_3)_3$, R^1 = H
6 R = H, R^1 = CH_2CH_3
7 R = C_6H_5, R^1 = H
8 R = $(CF_2)_2CF_3$, R^1 = H
9 R = R^1 = H
10 R = CH_3, R^1 = H
11 R = CF_3, R^1 = H
17 R = CH_2CH_3, R^1 = H
18 R = $CH(CH_3)_2$, R^1 = H

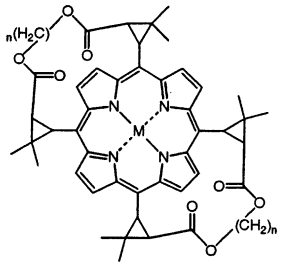

12 n = 8 (**a**), 9 (**b**), 10 (**c**), 11 (**d**), 12 (**e**), 14 (**f**), 16 (**g**)

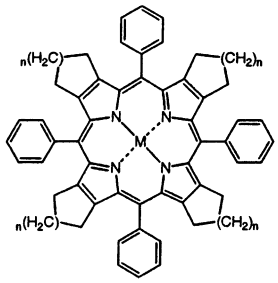

14 n = 1
15 n = 2
16 n = 3

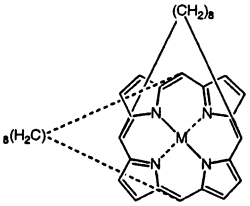

19

significant changes in the chemical and spectroscopic properties of the porphyrin macrocycle.[1,6,7] Chemical properties that are known to be modified by nonplanar distortion include oxidation potentials, basicity of the inner nitrogen atoms, and axial ligand binding affinity,[1,6−9] all of which can influence the biological function of porphyrin cofactors in proteins. In nonbiological applications of porphyrins, host−guest interactions[10,11] and the enantioselectivity of catalytic epoxidation[12] can be fine-tuned by nonplanar deformations.

Several spectral signatures of the porphyrin macrocycle have been shown to be significantly affected by substituent-induced nonplanar deformations, including those detected by resonance Raman, ^{1}H NMR, and UV−visible spectroscopies.[1,6,7] In the present work, we examine the origin of the red shifts seen in the optical spectra of nonplanar porphyrins, in particular for peripherally crowded nonplanar porphyrins such as **1**−**5**. This is a topic that has recently generated considerable debate in the literature.[13−16] The connection between absorption band red shifts and nonplanar deformations of the porphyrin macrocycle is important from a theoretical standpoint and also because this spectral correlation might be used to probe the structures of hemes (iron porphyrins), chlorophylls and related photosynthetic pigments, and other tetrapyrrole cofactors in proteins. Nonplanar heme distortion has recently been recognized to be a conserved structural feature of some proteins and thus provides a mechanism by which biochemical function of the heme may be altered by its protein environment.[17−19]

The first analysis of the relationship between nonplanarity and red shifts in the optical spectra of peripherally crowded nonplanar porphyrins was in a study of zinc octaethyltetraphenylporphyrin [ZnOETPP, **1** (M = Zn)].[20] The optical spectrum of ZnOETPP showed a large red shift compared to zinc octaethylporphyrin [ZnOEP, **6** (M = Zn)] or zinc tetraphenylporphyrin [ZnTPP, **7** (M = Zn)]. Semiempirical (INDO/S) calculations indicated that this resulted from a greater destabilization of the highest occupied molecular orbital (HOMO) than of the lowest unoccupied molecular orbital (LUMO) in ZnOETPP compared to ZnOEP and ZnTPP. Consistent with

(4) Ema, T.; Senge, M. O.; Nelson, N. Y.; Ogoshi, H.; Smith, K. M. *Angew. Chem., Int. Ed. Engl.* **1994**, *33*, 1879.
(5) Jentzen, W.; Hobbs, J. D.; Simpson, M. C.; Taylor, K. K.; Ema, T.; Nelson, N. Y.; Medforth, C. J.; Smith, K. M.; Veyrat, M.; Mazzanti, M.; Ramasseul, R.; Marchon, J.-C.; Takeuchi, T.; Goddard, I. W. A.; Shelnutt, J. A. *J. Am. Chem. Soc.* **1995**, *117*, 11085.
(6) Ravikanth, M.; Chandrashekar, T. K. *Struct. Bonding (Berlin)* **1995**, *82*, 105.
(7) Shelnutt, J. A.; Song, X.-Z.; Ma, J.-G.; Jia, S.-L.; Jentzen, W.; Medforth, C. J. *Chem. Soc. Rev.* **1998**, *27*, 31.
(8) Shelnutt, J. A.; Medforth, C. J.; Berber, M. D.; Barkigia, K. M.; Smith, K. M. *J. Am. Chem. Soc.* **1991**, *113*, 4077.
(9) Jia, S. L.; Zhang, J.; Ema, T.; Nelson, N. Y.; Ma, J. G.; Medforth, C. J.; Smith, K. M.; Shelnutt, J. A., in preparation.
(10) Mazzanti, M.; Marchon, J.-C.; Shang, M.; Scheidt, W. R.; Jia, S.; Shelnutt, J. A. *J. Am. Chem. Soc.* **1997**, *119*, 12400.
(11) Muzzi, C. M.; Medforth, C. J.; Smith, K. M.; Jia, S.-L.; Shelnutt, J. A. *Chem. Commun.* **2000**, 131.
(12) Gazeau, S.; Pécaut, J.; Haddad, R. E.; Shelnutt, J. A.; Marchon, J.-C. *Eur. J. Inorg. Chem.* **2002**, 2956.
(13) DiMagno, S. G.; Wertsching, A. K.; Ross, C. R. *J. Am. Chem. Soc.* **1995**, *117*, 8279.
(14) Parusel, A. B. J.; Wondimagegn, T.; Ghosh, A. *J. Am. Chem. Soc.* **2000**, *122*, 6371.
(15) Wertsching, A. K.; Koch, A. S.; DiMagno, S. G. *J. Am. Chem. Soc.* **2001**, *123*, 3932.
(16) Ryeng, H.; Ghosh, A. *J. Am. Chem. Soc.* **2002**, *124*, 8099.
(17) Jentzen, W.; Song, X. Z.; Shelnutt, J. A. *J. Phys. Chem. B* **1997**, *101*, 1684.
(18) Jentzen, W.; Ma, J. G.; Shelnutt, J. A. *Biophys. J.* **1998**, *74*, 753.
(19) Hobbs, J. D.; Shelnutt, J. A. *J. Protein Chem.* **1995**, *14*, 19.
(20) Barkigia, K. M.; Chantranupong, L.; Smith, K. M.; Fajer, J. *J. Am. Chem. Soc.* **1988**, *110*, 7566.

this interpretation, ZnOETPP was easier to oxidize than ZnOEP or ZnTPP, but the first reduction potential did not change as significantly, confirming a narrowing of the HOMO−LUMO separation. Additional experimental data and semiempirical (INDO/S) calculations for a wide range of peripherally crowded nickel porphyrins including NiOETPP (**1**, M = Ni)[21] and NiT(*t*Bu)P (**5**, M = Ni)[5] reinforced this view. While it has been noted that the observed red shifts depend both on the substituents present on the porphyrin ring and on the amount and type of substituent-induced nonplanar deformation,[22] it has become generally accepted that a large red shift in the UV−visible bands is indicative of a very nonplanar porphyrin macrocycle.[1,6,7] That the red shifts are a consequence of nonplanarity and not the bulky substituents themselves is supported by studies of less sterically crowded NiOEP. NiOEP exists as a mixture of planar and nonplanar forms in solution with the nonplanar form exhibiting red-shifted absorption bands.[23,24]

In the first of several recent papers concerning the red-shift/nonplanarity connection, DiMagno[13] reported that the cobalt(II) complex of 5,10,15,20-tetrakis(heptafluoropropyl)porphyrin [CoT(C_3F_7)P, **8** (M = Co^{II})] was very saddle distorted, as demonstrated by X-ray crystallography, but apparently did not show a red shift in solution or in the solid-state. Theoretical (AM1) calculations were reported which showed that constraining porphine [H_2P, **9** (M = 2H)] to a saddled geometry actually produced a blue shift for the Q(0,0) band, the lowest energy $\pi-\pi^*$ transition. Based on these findings, it was suggested that the red shifts previously seen in nonplanar porphyrins were the result of different substituent effects in planar versus sterically crowded nonplanar porphyrins and, more specifically, the overlap of the aryl substituents in porphyrins **1**−**3** with the π-system of the porphyrin macrocycle. However, this hypothesis is clearly contradicted by the observation of large red shifts for strongly ruffled H_2T(*t*Bu)P **5**[4,25,26] and the nickel complex of 2,3,7,8,12,13,17,18-octaethyl-5,10,15,20-tetrabutylporphyrin.[27] The DiMagno paper was subsequently rebutted in a density functional theory (DFT) study of *ruf* and *sad* zinc porphyrins by Ghosh,[14] who calculated red shifts for both types of deformation. This latter finding was in agreement with the prevailing view that nonplanar distortions cause the large red shifts seen in the optical spectra of porphyrins.[1,6,7] It is important to note that the porphine macrocycle structure used in Ghosh's 2000 paper came from energy-optimized structures generated with the *un-truncated* macrocycle substituents, i.e., the whole substituent group.

Another paper by DiMagno[15] then used DFT to examine structural and electronic contributions to the electronic spectra of H_2P, tetramethylporphyrin [H_2T(Me)P] **10** (M = 2H)] and tetrakis(trifluoromethyl)porphyrin [H_2T(CF_3)P, **11** (M = 2H)]. In this study, the contribution arising from nonplanarity was estimated by artificially constraining the porphyrin into progressively more ruffled conformations. It was again concluded that nonplanarity (in this case ruffling) had a negligible effect on the electronic spectrum, and the major contributor to the red shift was now proposed to be in-plane nuclear reorganization (IPNR). IPNR was defined as changes in the porphyrin bond lengths and bond angles induced by interactions between the substituent and the porphyrin macrocycle. Most recently, another paper was published by Ghosh[16] confirming that neither artificially ruffling nor artificially saddling the porphyrin produces a large red shift. Based on these findings, it was concluded[16] that IPNR rather than nonplanarity was indeed the dominant effect.

As one of the groups originally proposing the red-shift/nonplanarity relationship,[5,8,21−23] we were intrigued by these new findings. The fact that a porphyrin can apparently be deformed into a very nonplanar structure but not show a large red shift is startling and potentially draws into question the origin of the red shifts in highly substituted nonplanar porphyrins. However, assessment of the importance of IPNR using the published work[15,16] was confounded by the lack of specific information about which substituent-induced changes in bond lengths and/or bond angles might produce the supposed IPNR red shift. Thus, it seemed that while an important question might have been raised about the origin of the red shift, the IPNR explanation for the missing red shift had not been adequately verified. We therefore decided to investigate the effect of structural perturbations on the electronic transitions of porphyrins in more detail, with the goals of understanding why the observed red shifts could not be reproduced by the constrained porphyrin structures and determining their true origin.

The highly nonplanar porphyrin MT(*t*Bu)P (**5**, M = Ni or H_2) and the less sterically hindered MT(Me)P (**10**, M = Ni or H_2) examined in our earlier work[5] provide the focus of our current computational studies because their meso alkyl substituents have similar electronic influences and produce nearly pure *ruf* deformations. Moreover, the observed red shift and nonplanar deformation in MT(*t*Bu)P is very large. In the present work, a molecular mechanics (MM) force field[8,28] that has been optimized for porphyrins is used to generate the requisite porphyrin structures, and semiempirical (INDO/S) quantum calculations based on the MM structures are used to calculate the corresponding electronic transitions.[5] The MM method used has been shown to accurately predict the X-ray structures of porphyrins[29] and INDO/S calculations are known to accurately reproduce the red shifts seen in peripherally crowded nonplanar porphyrins.[8,21]

One problem with studying the effects of nonplanarity, and therefore understanding how it influences the optical properties of the porphyrin macrocycle, is accurately defining the amounts and types of nonplanar deformation present in the porphyrin system. In early crystallographic studies of porphyrins, both *sad* and *ruf* deformations were generally referred to as ruffling, and more accurate definitions did not emerge until the work of Scheidt in the late 1980s.[2] Ruffling then took on a more specific meaning, namely, an alternate clockwise or anticlockwise

(21) Sparks, L. D.; Medforth, C. J.; Park, M.-S.; Chamberlain, J. R.; Ondrias, M. R.; Senge, M. O.; Smith, K. M.; Shelnutt, J. A. *J. Am. Chem. Soc.* **1993**, *115*, 581.
(22) Medforth, C. J.; Senge, M. O.; Smith, K. M.; Sparks, L. D.; Shelnutt, J. A. *J. Am. Chem. Soc.* **1992**, *114*, 9859.
(23) Alden, R. G.; Crawford, B. A.; Doolen, R.; Ondrias, M. R.; Shelnutt, J. A. *J. Am. Chem. Soc.* **1989**, *111*, 2070.
(24) Jentzen, W.; Unger, E.; Karvounis, G.; Shelnutt, J. A.; Dreybrodt, W.; Schweitzer-Stenner, R. *J. Phys. Chem.* **1996**, *100*, 14184.
(25) Senge, M. O.; Ema, T.; Smith, K. M. *J. Chem. Soc., Chem. Commun.* **1995**, 733.
(26) Somma, M. S.; Medforth, C. J.; Nelson, N. Y.; Olmstead, M. M.; Khoury, R. G.; Smith, K. M. *Chem. Commun.* **1999**, 1221.
(27) Senge, M. O.; Renner, M. W.; Kalisch, W. W.; Fajer, J. *J. Chem. Soc., Dalton Trans.* **2000**, 381.
(28) Song, X.-Z.; Jentzen, W.; Jaquinod, L.; Khoury, R. G.; Medforth, C. J.; Jia, S.-L.; Ma, J.-G.; Smith, K. M.; Shelnutt, J. A. *Inorg. Chem.* **1998**, *37*, 2117.
(29) Shelnutt, J. A. In *The Porphyrin Handbook*; Kadish, K. M., Smith, K. M., Guilard, R., Eds.; Academic Press: Boston, 2000; Vol. 7, p 167.

twisting of the pyrrole rings such that the meso carbon atoms are displaced alternately above or below the porphyrin plane (see Figure 1). In contrast, saddling was defined as an alternate up or down tilting of the pyrrole rings of the porphyrin macrocycle. Recently, Shelnutt and co-workers have developed normal-coordinate structural decomposition (NSD)[17,18,29−31] as a method for identifying and quantifying the out-of-plane and in-plane distortions of tetrapyrroles. In the NSD analysis, distortions are represented in terms of the vibrational modes of the molecule. For example, the ruffling and saddling deformations observed in crystal structures correspond to the two lowest-frequency out-of-plane B_{1u} and B_{2u} vibrational modes of the porphyrin macrocycle;[17] these are the softest deformation types, explaining why they are so commonly observed in porphyrin crystal structures. The NSD analysis determines the contribution of all 66 in-plane and out-of-plane normal coordinates of the macrocycle to a distorted porphyrin structure, although just the displacements for the six lowest frequency (softest) out-of-plane deformations are depicted in Figure 1 to graphically illustrate the NSD method. Interestingly, a combination of just these six normal-coordinate deformations frequently provides a reasonably accurate picture of the out-of-plane distortion of the porphyrin. In the present study, NSD is used extensively to obtain a detailed analysis of the deformations present in the calculated porphyrin structures. As we will show later, the ability to accurately quantify *all* of the out-of-plane deformations making up the distortion (not just the six deformations of Figure 1) is crucial to obtaining a full understanding of the origins of the red shifts seen for the nonplanar porphyrins and to obtaining an explanation of why large red shifts are not seen for the artificially constrained nonplanar structures.

Our studies of the tetraalkylporphyrins show that disentangling the various contributions to the optical spectra is made possible by using a well-controlled porphyrin series and the combined computational tools of normal-coordinate structural decomposition, INDO/S semiempirical quantum calculations, and molecular mechanics and dynamics calculations. In agreement with the previous DFT results,[15,16] the combined MM/INDO method predicts only a small red shift when the porphyrin macrocycle is artificially ruffled. Several mechanisms are then considered to explain the remaining red shift, including the previously proposed IPNR effect. Our study of a series of nickel and zinc tetraalkylporphyrins indicates that the large red shifts seen for these peripherally crowded porphyrins are primarily the result of out-of-plane deformations, as is generally accepted,[1,6,7] but that surprisingly all of the ruffling-symmetry deformations shown in Figure 2 contribute significantly to the UV−visible band shifts. The importance of these nonplanar deformations in producing red shifts is then experimentally demonstrated by using the series of bridled chiroporphyrins **12a**−**g**.

Materials and Methods

Molecular Mechanics (MM), Molecular Dynamics (MD), and INDO/S Calculations and Normal-Coordinate Structural Decomposition (NSD). Molecular mechanics calculations using Cerius2 version 4.6 software (Accelrys Inc., San Diego) were carried out and displayed on a Silicon Graphics Octane workstation. The force field used in the calculations is based on DREIDING II,[32] modified to include force constants and equilibrium values for bonds, angles, torsions, and improper torsions as well as parameters describing the van der Waals and electrostatic interactions for the atoms of the porphyrin macrocycle,[8] and including the most recent revisions of these parameters.[28] For the tetraalkylporphyrin INDO/S calculations, energy-optimized structures with and without various constraints and fixed atoms were generated.

To determine the magnitude of the normal-coordinate deformations for solution structures of the bridled chiroporphyrins, six molecular dynamics trajectories were obtained for 2-ns intervals at a fixed temperature of 300 K. Previous to running the dynamics calculations, the chiroporphyrin structures were built and equilibrated by running at least 100 ps of dynamics at an elevated temperature of 900 K (500 ps at 600 K for the eight- and nine-carbon strap chiroporphyrins). Snapshot structures extracted from the 2-ns MD trajectories at 0.10- or 0.05-ps intervals were then analyzed by normal-coordinate structural decomposition.[17,18] The individual deformations for all 20 000 (or 40 000) snapshot structures from each trajectory were then averaged to determine the average degree of nonplanar deformation in the two lowest-frequency deformation modes of each out-of-plane symmetry type and the two lowest-frequency modes of each in-plane symmetry type (24 modes total). The values reported are averages over the six independent 2-ns dynamics trajectories starting from different initial structures and velocities, obtained by additional MD simulations at elevated temperatures followed by cooling to 300 K. These time-averaged deformations give a measure of the distortion under solution

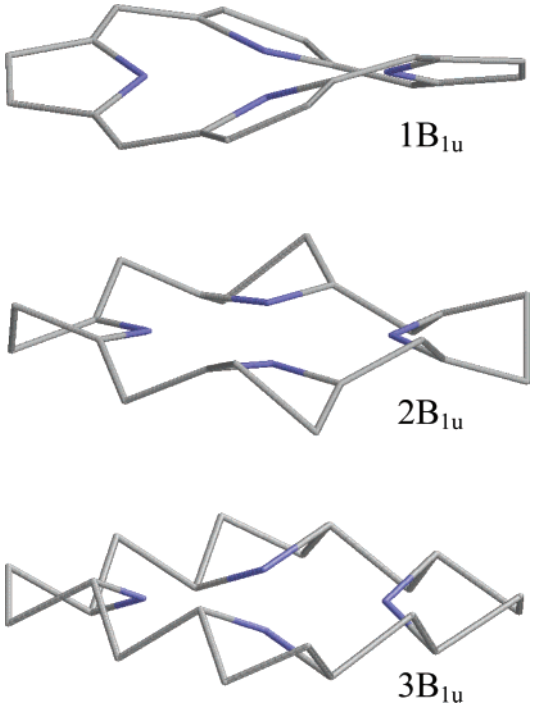

Figure 2. B_{1u} normal coordinates of the porphyrin macrocycle. The frequency of the $1B_{1u}$ deformation is the lowest (88 cm^{-1}), and the frequencies of the $2B_{1u}$ (516 cm^{-1}) and $3B_{1u}$ (727 cm^{-1}) deformations are much higher. Thus, using the harmonic approximation and the frequencies given, a deformation along the $2B_{1u}$ mode requires 34.5 times the strain energy of an equivalent deformation along the $1B_{1u}$ normal coordinate. A 2-Å deformation or displacement is shown for each normal coordinate, although such a large displacement for the high-order modes would never be observed experimentally because of the extreme strain energy required to produce the deformation.

(30) NSD data for more than 1500 hemes of protein structures contained in the Protein Data Bank are available in reference 29.
(31) A web-based version of the NSD program is available at http://jasheln.unm.edu. Sun, L.-S.; Jentzen, W.; Shelnutt, J. A., Sandia National Laboratories: Albuquerque, NM, 2002.
(32) Mayo, S. L.; Olafson, B. D.; Goddard, W. A. I. *J. Phys. Chem.* **1990**, *94*, 88.

conditions by averaging over the many conformations of the flexible portions of the chiroporphyrins.

NSD analysis of the MD snapshot structures was done with a C version of the NSD program originally written by Jentzen[17,18] and modified by Sun[31] to provide automation for processing multiple related structures. NSD analyses of the MM structures were carried out with a JAVA program based on the original C and MathCad (MathSoft Inc., Cambridge, MA) versions of the NSD program described by Jentzen and co-workers in detail elsewhere.[17,18] The web-based NSD computational engine based on the JAVA version is available for general use at http://jasheln.unm.edu.[31]

INDO/S calculations were performed by using HyperChem 5 software (HyperCube Inc., Gainesville, FL) after altering the nickel β_d parameter as described previously.[5] Where comparisons between our MM/INDO calculations and DFT calculations could be made, the band shifts predicted are similar, e.g., both techniques correctly predict large red shifts for nonplanar macrocycles generated by steric repulsion of peripheral substituent groups rather than internal constraints.[5,14,21]

Spectroscopy. UV−visible spectra of bridled chiroporphyrin complexes **12a**−**g** (M = Ni, 2H) were measured on approximately 2 μM CS_2 or CH_2Cl_2 solutions in a 1-cm quartz cell with either a Perkin-Elmer Lambda 9 or a Hewlett-Packard HP9852A spectrophotometer. The spectrometer resolution is approximately 2 nm. Curve fitting indicates the presence of at least two structural forms or two electronic transitions making up the Soret band. To get a single value for the peak wavelength of the Soret band, a second-order polynomial is fit to the five points near the maximum and interpolated to get the λ_{max} values reported.

Raman spectra were obtained from the porphyrins **12a**−**g** (M = Ni) in carbon disulfide or methylene chloride (2−100 μM) in 3 × 3 × 30 mm quartz cells at room temperature. The spectra were excited by using the 406.7-nm line of a model 304 Kr^+ laser (Coherent Inc.). Spectra were detected with a 0.75-m monochromator with a CCD detector system (JY Inc., Edison, NJ) described previously.[34] Peak frequencies were obtained by simulation of the spectra using Lorentzian line shapes and the program PeakFit (SPSS, Inc., Chicago, IL).

^{1}H NMR spectra of **12a**−**g** (M = 2H, Ni, Zn) were measured on Bruker AC 200 (Bruker-Biospin, S. A., Wissembourg, France) and Varian Avance 400 (Varian, Inc., Palo Alto, CA) spectrometers as described previously.[12] Electrospray mass spectra were obtained with a Finnigan MAT LCQ spectrometer (Thermo Finnigan, San Jose, CA).[12]

X-ray Crystallography. Single crystals suitable for X-ray analysis were obtained by slow evaporation of solutions of the complexes in various solvent mixtures: chloroform/acetonitrile (**12a** (M = Ni), monoclinic); dichloromethane/methanol/*n*-hexane (**12a** (M = Ni), orthorhombic); acetone/*n*-hexane (**12c** (M = Ni), monoclinic); acetone/*n*-heptane (**12c** (M = Ni), orthorhombic). Dark red crystals of the complexes were mounted on glass needles. Graphite monochromated Mo Kα radiation (λ = 0.710 73 Å) was used throughout. Intensity data were collected at 193(2) K on a Bruker SMART CCD detector (Bruker-AXS, GmbH, Karlsruhe, Germany). Data collection was performed by a hemisphere run taking frames (30 s) at 0.30° in ω. The data were corrected for Lorentz and polarization effects. A semiempirical absorption correction was carried out by using the program SADABS.[35] The structures were solved by direct methods and Fourier difference methods performed on a Silicon Graphics workstation, using the Bruker ShelXTL[36] software package for solution, refinement, and artwork. Neutral atom scattering factors were used).[33] Non-hydrogen atoms were located by Fourier difference methods, and they were refined anisotropically except when otherwise indicated. Hydrogen atoms were placed at calculated positions and refined as riding atoms with isotropic displacement parameters. Due to the large values of the thermal parameters and/or disorder of some carbon atoms of the bridles, it was necessary to take special precautions during the refinement cycles, as explained in Text S1 of the Supporting Information. Crystallographic data in CIF format is available as Supporting Information.

Scheme 1. Synthesis of the Bridled Chiroporphyrin Free Bases **12a**−**g** (M = 2H)

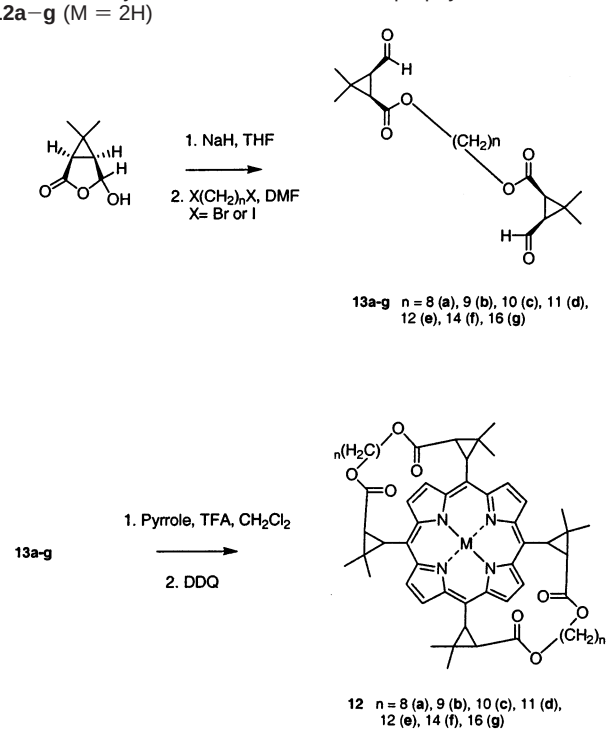

Synthesis. Deprotonation of (1*R*)-*cis*-hemicaronaldehyde (biocartol) by sodium hydride, followed by nucleophilic attack on a dihalogenoalkane of appropriate length, led to the dialdehydes **13a**−**g** in 50−99% yield (Scheme 1). The latter were condensed with pyrrole according to a literature method[37] to afford the bridled chiroporphyrins **12a**−**g** (M = 2H) in 3−12% yield.

Synthesis of Dialdehydes 13a−g Using 13a As an Example. NaH (1.13 g, 28 mmol) was added in small portions to a dry THF (30 mL) solution of biocartol (4 g, 28 mmol) under argon at 10 °C. The mixture was then stirred for 30 min at room temperature and 1.4 mL of 1,8-diiodooctane (1.4 mL, 7 mmol) in dry DMF (120 mL) was added. After stirring for 24 h under argon at room temperature, diethyl ether was added and the organic layer was washed and dried over Na_2SO_4. The solvent was then removed under reduced pressure. The residue was purified by silica gel chromatography using methylene chloride/methanol (97:3) to afford 2.76 g of **13a** as a colorless oil in quantitative yield. Analytical data for **13a**−**g** are given in Text S2 of the Supporting Information.

Synthesis of Free Base Bridled Chiroporphyrins 12a−g (M = 2H) Using 12a (M = 2H) As an Example. Degassed methylene chloride (1.9 L) containing **13a** (M = 2H) (3.27 g, 8.3 mmol), pyrrole (1.4 mL, 20 mmol), and TFA (1.53 mL, 20 mmol) was stirred at room temperature under argon for 6 days. The reaction mixture was diluted 3 times with methylene chloride and then oxidized with DDQ (1.26 g, 16.6 mmol). After stirring for 4 h the solvent was removed under reduced pressure. The residue was chromatographed on an alumina column eluted with methylene chloride/methanol (98:2) and then on silica gel plates eluted with the same solvent mixture. The porphyrin **12a** (M = 2H) was obtained as a purple solid in 5% yield. Analytical data for **12a**−**g** (M = 2H) are given in the Supporting Information.

Synthesis of Nickel Complexes 12a−g (M = Ni) Using 12a (M = Ni) As an Example. $NiCl_2 \cdot 6H_2O$ (63 mg, 0.266 mmol) in ethanol

(33) International Tables for X-ray Crystallography, Kynoch Press: Birmingham, England.
(34) Franco, R.; Ma, J. G.; Lu, Y.; Ferreira, G. C.; Shelnutt, J. A. *Biochemistry* **2000**, *39*, 2517.
(35) Sheldrick, G. M., Ed., Universität Göttingen, 1994.
(36) Sheldrick, G. M., Ed., SHELXTL-Plus, Version 5.1: Structure Determination Software Programs; Bruker Analytical X-ray Instruments Inc.: Madison, WI, 1998.

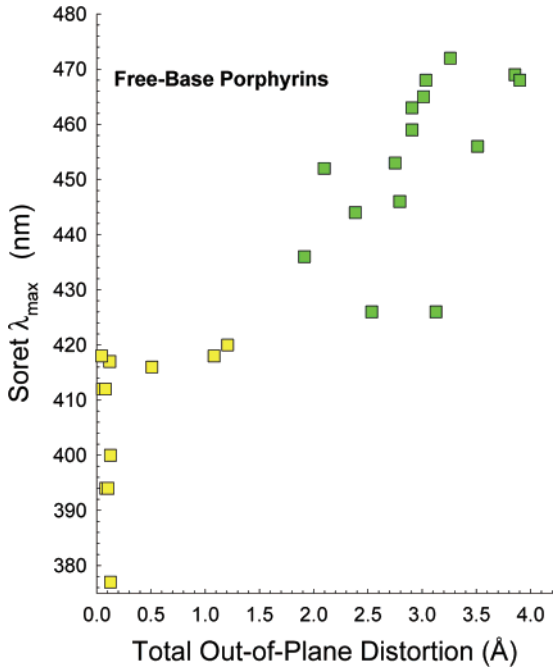

Figure 3. Soret band wavelengths observed in methylene chloride solutions versus the ruffling deformation obtained by NSD from the X-ray crystal structures of the free-base porphyrin. A similar plot for nickel porphyrins is given in Figure S1 of the Supporting Information. Yellow filled boxes are porphyrins with little or no peripheral steric crowding; green filled points are highly sterically crowded porphyrins. The data plotted is listed in Tables S2 to S5 of the Supporting Information.

(3 mL) was added to **12a** (M = 2H) (13 mg, 0.013 mmol) in chloroform (3 mL). The mixture was stirred under reflux for 20 h. The solvent was removed under reduced pressure and the residue was purified on a silica gel column eluted with methylene chloride to provide 12 mg (88%) of **12a** (M = Ni). Analytical data for **12a**−**g** (M = Ni) are given in the Supporting Information.

Synthesis of Zinc Complexes 12a−g (M = Zn) Using 12a (M = Zn) As an Example. $Zn(OAc)_2 \cdot 2H_2O$ (123 mg, 0.560 mmol) in ethanol (20 mL) was added to a solution of **12a** (M = 2H) (55 mg, 0.056 mmol) in chloroform (20 mL). The mixture was stirred at room temperature for 24 h. The solvent was removed under reduced pressure and the residue was purified on a silica gel column eluted with methylene chloride to afford 53 mg (91% yield) of **12a** (M = Zn). Analytical data for **12a**−**g** (M = Zn) are given in the Supporting Information.

Results and Discussion

Red Shifts of the UV−Visible Bands of Peripherally Crowded Porphyrins. Figure 3 (free base porphyrins) and Figure S1 of the Supporting Information (nickel complexes) summarize some UV−visible spectral and X-ray structural data relevant to the red-shift phenomenon in nonplanar porphyrins. The experimental data compiled to provide Figures 3 and S1 are given in Tables S2−S5 of the Supporting Information. Tables S2−S5 give the wavelengths of the Soret bands, the Q(0,0) bands, the total out-of-plane deformations d_{total} (calculated from the crystal structures using NSD), and an estimation of the electronic effect of the peripheral substituents (obtained by summing the Hammett constants σ_p for the substituents). In Figure 3, the planar-to-moderately nonplanar compounds ($d_{total} < \sim 2$ Å) are mostly porphyrins such as OEP and TPP that lack substantial steric crowding of peripheral substituents. Some dodecasubstituted porphyrins, such as porphyrin **14**, are also included in this group as their substituents are known not to cause large nonplanar deformations.[8,38,39] The group of highly sterically crowded porphyrins, in contrast, exhibit large total distortions ($d_{total} > \sim 2$ Å) and have strongly red-shifted absorption bands relative to the group of more planar porphyrins.

In Figure 3 (and in Figure S1), there is considerable scatter evident in the wavelengths of the absorption maxima (typically about 40 nm) for the B(0,0) (Soret) band for both the planar-to-moderately nonplanar porphyrins and the highly nonplanar porphyrins. The large range of Soret absorption maxima within a group is likely related to several factors, including the electron donating/withdrawing effect of the substituents, the number of substituents, and the amount and type of nonplanar deformation. However, despite the scatter, there is little overlap of the absorption maxima or of the total out-of-plane deformations for the two groups of porphyrins, indicating a strong red shift for the peripherally crowded and highly nonplanar porphyrins. In other words, this red shift appears to be large enough that it is not obscured either by variation of the type and number of substituents or by metal substitution in the core (M = 2H or Ni).

The presence of a large red shift for peripherally crowded nonplanar porphyrins has also been confirmed by a number of studies where the electronic effect of the substituents is more carefully controlled for a series of porphyrins. The two most relevant studies vary the size of rings fused to the pyrrole position of dodecasubstituted porphyrins (**14**−**16**)[8,38,39] or the bulkiness of alkyl substituents at the meso positions (**10**, **17**, **18,** and **5**).[5] The UV−visible data for these mostly saddled (**14**−**16**) or ruffled (**10**, **17**, **18,** and **5**) porphyrins are summarized in Table S6, and data for the latter series are plotted in Figure 4. Progressively larger red shifts occur with increasing steric crowding of the substituents for both classes of porphyrin. The trends are more clearly seen for these series of porphyrins because the number and nature of the substituents and the type of distortion (e.g., saddle versus ruffle, as determined crystallographically and/or by molecular modeling studies) is constant within each series. Note that the trends for the ruffled series (**14**−**16**) and the saddled series (**10**, **17**, **18**, and **5**) are similar even though the numbers and types of substituent and the types of deformation are markedly different for the two series.

MM and INDO/S Calculations for Tetraalkylporphyrins. The data in Figure 3, Figure S1, Table S6, and Figure 4 provide clear experimental evidence for a very large red shift arising from steric crowding of the peripheral substituents. The important question is whether the observed UV−visible band red shifts are a consequence of the out-of-plane deformations that accompany peripheral steric crowding, as generally accepted,[1,6,7] or whether they are the result of some other effect such as IPNR.[15,16] To answer this question, we began by calculating energy-minimized MM structures for porphine and several tetraalkylporphyrins containing Zn or Ni. Using these MM structures, we then calculated $\pi-\pi^*$ electronic transition energies via the INDO/S method. Table S7 of the Supporting Information summarizes the ruffling dihedral angles and wavelengths of the UV−visible bands that are calculated using the

(37) Wagner, R. W.; Johnson, T. E.; Lindsey, J. S. *Tetrahedron* **1997**, *53*, 6755.
(38) Medforth, C. J.; Berber, M. D.; Smith, K. M.; Shelnutt, J. A. *Tetrahedron Lett.* **1990**, *31*, 3719.
(39) Senge, M. O.; Medforth, C. J.; Sparks, L. D.; Shelnutt, J. A.; Smith, K. M. *Inorg. Chem.* **1993**, *32*, 1716.

Table 1. Results of INDO/S Calculations on Molecular Mechanics Structures for Nickel and Zinc Tetraalkylporphyrins

		nickel			zinc		
entry	description of structure	ruffling angle,[a] deg	*B*(0,0),[b] nm	δ,[c] deg	ruffling angle,[a] deg	*B*(0,0),[b] nm	δ,[c] deg
1A	T(Me)P unconstrained energy minimization	38	354.6	3.0	19	348.6	−0.8
1B	T(*t*Bu)P unconstrained energy minimization	56	395.9	0.6	44	397.1	1.3
2	T(Me)P Me on *t*Bu vector of T(*t*Bu)P and Me geometry optimized	56[d]	391.2	0.6	44	391.4	0.0
3A	T(Me)P constrained ruffled and energy minimized	56[d]	361.0	−4.6	44	355.9	−3.3
3B	T(Me)P constrained ruffled and energy minimized	60[d]	363.3	−5.5			
4A	T(Me)P *with* constrained T(*t*Bu)P bond lengths	60[d]	363.4	−5.3			
4B	T(Me)P with T(*t*Bu)P bond lengths and $C_\alpha-C_m-C_\alpha$ bond angles	60[d]	362.8	−6.1			
4C	T(Me)P constrained planar and minimized	0[d]	341.9	0.2			
4D	T(*t*Bu)P constrained planar and minimized	0[d]	336.9	0.0			
5	T(Me)P Me constrained to $C_\alpha-C_\alpha-C_m$ plane to correct for floppy methyl effect	56[d]	362.6	0.0	44	357.1	0.0
6A	T(Me)P ruffled by steric interactions at methyl groups	60	380.8	6.4			
6B	Compound **19** (ruffled using 8-carbon straps)	56	391.9	4.8	46	404.5	8.8
6C	T(Me)P constrained ruffled and $N-C_\alpha-C_m-C_\alpha$ torsion angle constrained to value of energy minimized T(*t*Bu)P	56[d]	380.4	−9.5	44	379.6	−8.6
7	T(Me)P with constrained $N-C_\alpha-C_m-C_\alpha$ torsion and corrected for droopy methyl effect	56[d]	388.0	0.0	44	387.3	0.0

[a] $C_\alpha-N-N-C_\alpha$ (trans) torsion angle. [b] Average of two closely spaced transitions. [c] δ is the bond angle that the meso substituent makes with the $C_\alpha-C_m-C_\alpha$ plane. Negative values indicate that the meso substituent is displaced toward the mean plane of the porphyrin and positive values are away from the mean plane. [d] Constrained structure optimization.

MM/INDO procedure for the nickel and zinc tetraalkylporphyrins and compares the calculated transition wavelengths with the observed spectral data.

The trends in the measured UV−visible absorption maxima of the Ni tetraalkylporphyrins with the degree of ruffling are shown in Figure 4, and we see that these experimental trends are clearly reproduced by the transition wavelengths given by the MM/INDO calculations. The scatter in Figure 4 is less, as would be expected, for this homologous series of porphyrins than that seen in Figure 3 for a more varied group of porphyrins. The calculations consistently overestimate the energies of the B(0,0) transitions (and underestimate the energies of the Q(0,0) transitions). Further, the INDO calculations predict a red shift of 2942 cm^{-1} for the Soret band of NiT(*t*Bu)P versus NiT(Me)P, which is in reasonable agreement but about 50% larger than the experimentally observed red shift of 1963 cm^{-1}. Similar results are obtained for the Zn(II) complexes, with a calculated red shift of 3504 cm^{-1} and an observed red shift of 2032 cm^{-1} (obtained by using the *n*-butyl complex as a reference instead of the methyl complex).[40] Nevertheless, the agreement is reasonable, so MT(Me)P and MT(*t*Bu)P (M = Ni or Zn) were chosen for more detailed studies of the factors causing the red shift (Tables 1 and 2). These two tetraalkylporphyrins are particularly good choices because the substituents have similar electronic effects and because there are fewer local minima for the substituent orientations than would be the case for less symmetrical ethyl or isopropyl substituents.

The out-of-plane deformations present in the energy-minimized structures of MT(*t*Bu)P and MT(Me)P (M = Ni or Zn) were analyzed by NSD and the deformations for the B_{1u} symmetry modes are given in Table 2 (entries 1A and 1B). (The corresponding totally symmetric in-plane deformations are provided in Tables S8 (Ni) and S9 (Zn) of the Supporting Information.) Smaller out-of-plane deformations are observed for Zn than for Ni, consistent with the metal-size dependence noted previously.[21,41] As expected, T(*t*Bu)P is much more nonplanar than T(Me)P as a result of the greater steric bulk of

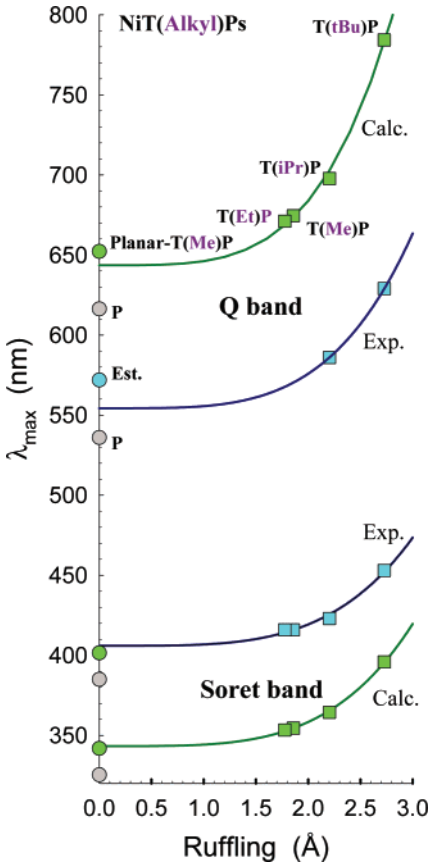

Figure 4. Absorption band wavelengths observed in dichloromethane solution (cyan) and calculated by using the MM/INDO method for the nickel tetraalkylporphyrins (green) and nickel porphine (gray circles). The curves can be approximated by the functional form $\lambda = a + b(d_{ruf})^4$, where *a* and *b* are least-squares fitting parameters. Only the data points indicated by squares are used in the least-squares fits, i.e., the NiP and planar-NiT(Me)P points are omitted for the fits.

the *tert*-butyl substituents (e.g., d_{total} = 1.87 Å in NiT(Me)P versus 2.75 Å in NiT(*t*Bu)P). For both porphyrins, essentially all of the calculated out-of-plane distortion (d_{total}) is localized in the B_{1u} ruffling-symmetry modes (B_{1u} total) and mainly in the first-order (lowest frequency) B_{1u} deformation ($1B_{1u}$) that is commonly referred to as ruffling. However, the second-order

(40) Senge, M. O.; Bischoff, I.; Nelson, N. Y.; Smith, K. M. *J. Porphyrins Phthalocyanines* **1999**, *3*, 99.
(41) Sparks, L. D.; Anderson, K. K.; Medforth, C. J.; Smith, K. M.; Shelnutt, J. A. *Inorg. Chem.* **1994**, *33*, 2297.

Table 2. Out-of-Plane Total and B_{1u} Deformations of Nickel and Zinc Tetraalkylporphyrin Molecular Mechanics Structures

	nickel						zinc					
entry[a]	ruffling angle,[b] deg	total d_{total}, Å	B_{1u}, Å	$1B_{1u}$, Å	$2B_{1u}$, Å	$3B_{1u}$, Å	ruffling angle, deg	total d_{total}, Å	B_{1u}, Å	$1B_{1u}$, Å	$2B_{1u}$, Å	$3B_{1u}$, Å
1A	38 (min)	1.8650	1.8642	1.8578	0.1397	0.0656	19 (min)	0.9703	0.9613	0.9546	0.1052	0.0411
1B	56 (min)	2.7499	2.7499	2.7290	0.3229	0.1012	44 (min)	2.2714	2.2714	2.2409	0.3566	0.1030
							X-ray[c]	*2.4707*	*2.3954*	*2.3903*	*0.1424*	*0.0647*
2	56 (fixed)	2.7499[d]	2.7499	2.7290	0.3229	0.1012	44 (fixed)	2.2714[d]	2.2714	2.2409	0.3566	0.1030
3A	56 (const)	2.5644	2.5643	2.5613	0.1180	0.0374	44 (const)	2.0377	2.0377	2.0352	0.0968	0.0267
3B	60 (const)	2.7063	2.7062	2.7037	0.1130	0.0265						
4A	60 (const)	2.7179	2.7178	2.7155	0.1068	0.0267						
4B	60 (const)	2.7467	2.7466	2.7423	0.1462	0.0429						
4C	0 (const)	0.0072	0.0007	0.0006	0.0003	0.0003						
4D	0 (const)	0.0016	0.0012	0.0012	0.0001	0.001						
5	56 (const)	2.5644[e]	2.5643	2.5613	0.1180	0.0374	44 (fixed)	2.0377[e]	2.0377	2.0352	0.0968	0.0267
6A	60 (sterics)	2.7704	2.7703	2.7667	0.0916	0.1077						
6B	56 (straps)	2.7168	2.7003	2.6884	0.2213	0.1243	46 (straps)	2.3792	2.3597	2.3413	0.2509	0.1542
6C	56 (tors)	2.7283	2.7282	2.7153	0.2335	0.1261	44 (tors.)	2.2705	2.2704	2.2520	0.2505	0.1425
7	56 (+Me)	2.7271	2.7270	2.7145	0.2277	0.1282	44(+Me)	2.2702	2.2701	2.2522	0.2444	0.1451

[a] Description of structure as in Table 1. [b] $C_\alpha-N-N-C_\alpha$ (trans) torsion angle. [c] Taken from the literature.[25] [d] Same as entry 1B (core unchanged). [e] Same as entry 1A (core unchanged).

$2B_{1u}$ and the third-order $3B_{1u}$ deformations (shown in Figure 2) are also significant irrespective of the porphyrin substituents and the central metal. The significance of these deformations is underscored when one considers the large deformation energies required to induce even small displacements for these high-order modes, given that the distortion energy depends on the square of the frequency of the out-of-plane mode (see caption of Figure 2).[17,18]

Figure S2A of the Supporting Information shows a plot of the $2B_{1u}$ and $3B_{1u}$ deformations versus the $1B_{1u}$ deformation for the calculated nickel tetraalkylporphyrin complexes. The $3B_{1u}$ deformation increases linearly with the amount of $1B_{1u}$ deformation. The linear relationship suggests an equal partitioning of strain energy into the $1B_{1u}$ and $3B_{1u}$ modes. In contrast, the $2B_{1u}$ deformation increases in a nonlinear fashion with $1B_{1u}$; the differences between the $2B_{1u}$ and $3B_{1u}$ contributions are discussed further below. The molecular mechanics structures on this point are in broad agreement with the X-ray crystallographic structures in that both data sets show deformations in these high-order modes and the deformations increase with increased ruffling, though the shapes of the curves and overall magnitudes are somewhat different in the two cases.

Crystallographic data have been reported for ZnT(*t*Bu)P(pyridine),[25] and NSD results for this structure are included in Table 2 (the complete NSD analysis is given in Table S18 of the Supporting Information). The crystal structure contains approximately the same amount of total nonplanar deformation and $1B_{1u}$ ruffling deformation seen in the molecular mechanics structure, with additional small saddling (B_{2u}) and doming (A_{2u}) deformations, probably due to the presence of an axial ligand and to crystal packing forces not included in the calculation. In agreement with the molecular mechanics calculations, significant $2B_{1u}$ and $3B_{1u}$ deformations are seen in the crystal structure of ZnT(*t*Bu)P(pyridine). However, the amount of these deformations is less than in the calculated structures, consistent with the dependence on the amount of $1B_{1u}$ deformation shown in Figure S2B for a wide variety of ruffled Ni porphyrin crystal structures. Nevertheless, it is clear that deformations in these high-frequency modes are present in nonplanar porphyrin crystal structures as they are in the calculated structures. We will return to the significance of these small but important higher order deformations in the following discussion.

The crystal structure of NiT(Me)P has also been reported[42−45] and is virtually planar ($d_{total} \sim 0.3$ Å), in contrast with the calculated structure that is considerably nonplanar ($d_{total} \sim 1.9$ Å). In agreement with the calculated structure, resonance Raman spectroscopic studies suggest that NiT(Me)P is nonplanar in solution.[5] This discrepancy is probably explained by crystal packing forces overcoming the shallow energy well favoring ruffling of NiT(Me)P.[5] A similar phenomenon has been noted for NiOEP, where both planar and nonplanar structures have been detected in solution and in the crystalline state.[23,46] The triclinic crystalline forms of NiOEP show essentially planar macrocycles ($d_{total} \sim 0.1$ Å), whereas the tetragonal form is ruffled ($d_{total} \sim 1.5$ Å).

Possible Origins of the Large Red Shifts in the UV−Visible Bands of Tetra(*tert*-butyl)porphyrin. The origins of the large red shifts of the UV−visible bands of MT(*t*Bu)P versus MT(Me)P (M = Ni or Zn) were investigated in more detail. The following discussion relates to the Soret band of the nickel complex, although similar results are obtained for the corresponding zinc complexes (Tables 1 and 2) and for the Q-bands of both metal complexes (e.g., Table S7). As noted above, the calculated red shift for NiT(*t*Bu)P versus NiT(Me)P is 2942 cm^{-1}. The difference between the substituent electronic effects for a *tert*-butyl group compared to a methyl group is expected to be small. This was confirmed by using a structure where the *tert*-butyl group in the energy-minimized structure of NiT(*t*Bu)P was replaced with a methyl group located along the same (C_m-C_1) vector, and then just the methyl group was energy minimized while constrained to move along and rotate about this orientation (entry 2 in Table 1). This methyl-substituted NiT(*t*Bu)P macrocycle shows a small blue shift (303 cm^{-1}) compared to energy-minimized NiT(*t*Bu)P as expected. This leaves a large calculated red shift of 2639 cm^{-1} that must be unrelated to a direct electronic effect of the different *meso* substituents.

(42) Kutzler, F. W.; Swepston, P. N.; Berkovitch-Yellin, Z.; Ellis, D. E.; Ibers, J. A. *J. Am. Chem. Soc.* **1983**, *105*, 2996.
(43) Gallucci, J. C.; Swepston, P. N.; Ibers, J. A. *Acta Crystallogr.* **1982**, *B38*, 2134.
(44) Ulman, A.; Gallucci, J.; Fisher, D.; Ibers, J. A. *J. Am. Chem. Soc.* **1980**, *102*, 6852.
(45) Nelson, N. Y., Ph.D. Thesis, University of California at Davis, 2000.
(46) Brennan, T. D.; Scheidt, W. R.; Shelnutt, J. A. *J. Am. Chem. Soc.* **1988**, *110*, 3919.

In the same procedure described for some previous DFT calculations,[15] $C_\alpha-N-N-C_\alpha$ dihedral angles across the ring were used to constrain the T(Me)P and P structures to various ruffling angles defined by these dihedral angles for the Ni and Zn derivatives. Table S10 of the Supporting Information gives the transition wavelengths for the UV−visible bands calculated by INDO/S for these constrained ruffled structures. Significant red shifts in the absorption bands are predicted as the macrocycle is ruffled both for porphine and tetramethylporphyrin; from the planar structure to the 60° ruffled one, the red shift in the Soret band is 20−22 nm for Ni and slightly less for Zn. However, when one considers that the ruffling dihedral angle for energy-optimized NiT(Me)P is 38° and that for NiT(*t*Bu)P it is 56°, then it is clear that the Soret red shift from this component cannot explain the experimentally observed value of 37 nm for NiT(*t*Bu)P versus NiT(Me)P (Table S7). In other words, while increasing the ruffling angle from 38° to 56° does produce a small 500-cm^{-1} red shift (as seen by comparing entries 1A and 3A of Table 1), it is far less than that required to explain the full calculated or observed red shift between MT(Me)P and MT(*t*Bu)P (M = Ni or Zn). The MM/INDO calculations for these constrained structures therefore agree with the results obtained from DFT calculations; i.e., artificially ruffling the macrocycle does not produce the large experimentally observed UV−visible band red shifts.[15] It also seems unlikely that the remaining red shift of 2138 cm^{-1} is related to the small underestimation of the $1B_{1u}$ ruffling for structure 3A compared to energy-minimized NiT(*t*Bu)P (see Table 2), but this effect was also evaluated by further over-ruffling the macrocycle using a constraint angle of 60° (entry 3B of Tables 1 and 2). This increases the amount of ruffling ($1B_{1u}$) deformation to more closely match that seen in the energy-minimized structure of NiT(*t*Bu)P ($1B_{1u} \sim 2.7$ Å) but resulted in only a small incremental red shift of 175 cm^{-1}. Thus, even after accounting for the electronic effect of the *tert*-butyl group (entry 2) and the $1B_{1u}$ ruffling deformation (entry 3B), there is still a large 1963 cm^{-1} red shift to be explained.

Previous studies have attributed the missing Soret red shift to changes in the bond lengths and angles of the macrocycle caused by the substituents, termed in-plane nuclear reorganization or IPNR, but have not analyzed these effects in detail nor attempted to demonstrate that the bond lengths and bond angles actually change enough to cause the red shift.[15,16] Our analysis of the bond lengths and angles of energy-minimized NiT(Me)P and NiT(*t*Bu)P (Table S11 of the Supporting Information) did reveal significant structural differences which might conceivably be responsible for the red shifts. These changes included a pronounced decrease in the $C_\alpha-C_m-C_\alpha$ angle, an almost equally large increase in the $C_\beta-C_\alpha-C_m$ angle, and some small bond length changes. To evaluate the possible effects of these structural changes (IPNR), we investigated several energy-minimized constrained structures. In one calculation, the macrocycle bond lengths in NiT(Me)P with the correct amount of $1B_{1u}$ ruffling were fixed to the values in energy-minimized NiT(*t*Bu)P (entry 4A, Tables 1 and 2). In another calculation, both the bond lengths and the $C_\alpha-C_m-C_\alpha$ bond angles of NiT(Me)P were constrained at the values seen in the energy-minimized structure of NiT(*t*Bu)P (entry 4B). Neither of these constrained structures produced a significant red shift compared to the 60°-ruffled NiT(Me)P structure. Then, as a way of maximizing the IPNR, NiT(Me)P and NiT(*t*Bu)P were constrained to be planar

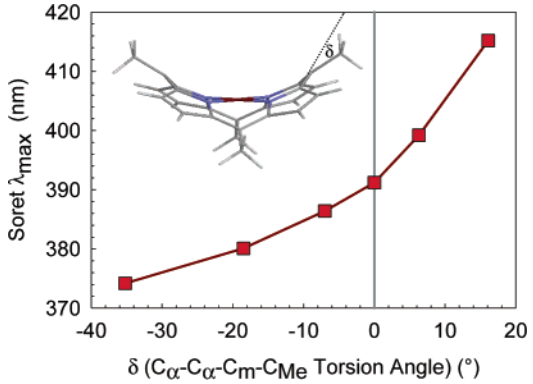

Figure 5. Illustration of the methyl group droop toward the macrocycle mean plane for NiT(Me)P artificially ruffled beyond its equilibrium geometry by constraining the $C_\alpha-N-N-C_\alpha$ dihedral angles (Inset) and the methyl droop effect on the wavelength of the Soret band for various methyl constraint angles relative to the $C_\alpha-C_m-C_\alpha$ plane. Note that the effect is enhanced for this structure because of the large out-of-plane displacements of the meso carbons in the NiT(*t*Bu)P porphyrin core (entry 1B of Tables 1 and 2), which was fixed in the calculations.

(entries 4C and 4D). IPNR must be much greater for planar NiT(*t*Bu)P and planar NiT(Me)P because steric interaction of the substituents with the macrocycle must be relieved entirely within the planar macrocycle. Further, because of the greater bulk of the *tert*-butyl substituents, IPNR must be tremendous for planar NiT(*t*Bu)P. These planar constrained structures do yield significant bond-length and bond-angle differences between the *tert*-butyl and methyl derivatives, with the pattern of bond length and angle differences being similar to but not the same as for the unconstrained nonplanar energy-minimized structures (Table S11). However, a large red shift is not observed for the planar constrained structure of NiT(*t*Bu)P relative to NiT(Me)P (Table 1); planar NiT(*t*Bu)P actually shows a blue shift compared to planar NiT(Me)P. These results suggest that, contrary to recent proposals,[15,16] IPNR is unlikely to be the origin of the missing Soret red shift in T(*t*Bu)P, although it may be important for other porphyrin systems. It should also be recognized at this point that significant bond-angle changes are expected for the nonplanar NiT(*t*Bu)P structure even without a direct substituent IPNR effect but instead as a natural consequence of the large torsion-angle changes associated with nonplanar distortion (see below).

What other factor or factors might explain the large red shifts for NiT(*t*Bu)P? One structural change apparent from the MM calculations is a tendency for the methyl groups in the overruffled NiT(Me)P structures to "droop" back toward the porphyrin plane. This substituent droop lowers the $C_\beta-C_\alpha-C_m-C_1$ torsion angle to near zero, minimizing this strain contribution. The structural change is made possible by the lack of significant steric repulsion between the methyl group and the macrocycle in the over-ruffled porphyrin. The alkyl group position relative to the $C_\alpha-C_m-C_\alpha$ plane is measured by the angle δ (i.e., the angle between the $C_\alpha-C_m-C_\alpha$ plane and the C_m-C_1 vector), which is given in Table 1. In the energy-minimized structures of NiT(Me)P and NiT(*t*Bu)P, the alkyl group is either in or slightly above the $C_\alpha-C_m-C_\alpha$ plane. In contrast, for the artificially ruffled energy-minimized constrained NiT(Me)P structures (entries 3A and 3B), the methyl groups droop toward the porphyrin plane ($\delta < 0$) as illustrated in the molecular mechanics structure shown in Figure 5; the steric

repulsion between the methyl and the porphyrin ring is simply not sufficient to hold the methyl above the $C_\alpha-C_m-C_\alpha$ plane.

A large blue shift arising from the methyl droop might explain why the constrained structures do not show the large red shifts. In other words, the absence of a large red shift could be an artifact of over-ruffling the porphyrin past its equilibrium geometry and an odd placement of the methyl groups, a structural effect most likely occurring in the DFT calculations as well.[15,16] Taking the 56°-constrained structure of NiT(Me)P and constraining the methyl group into the $C_\alpha-C_m-C_\alpha$ plane did produce an additional red shift (entry 5), but it was only 122 cm^{-1} and clearly insufficient to explain the missing red shift (1963 cm^{-1}). Nevertheless, circumstances might arise for which δ is large and this contribution might become significant. The curve in Figure 5, which was generated by constraining δ to different values using the fixed NiT(*t*Bu)P macrocycle (entry 1B), demonstrates that only small deformations from the $C_\alpha-C_m-C_\alpha$ plane are needed to cause significant shifts in the Soret band, especially for blue shifts caused by positive values of δ.

Red Shifts Resulting from the High-Order B_{1u} Deformations. The inability to generate significant red shifts using the mechanisms of IPNR or droopy substituents led us to more thoroughly investigate the significance of the small deformations in the $2B_{1u}$ and $3B_{1u}$ modes noted above. A significant role for the $2B_{1u}$ and $3B_{1u}$ deformations would explain why INDO/S[5,21] (and presumably DFT)[14] calculations on nonplanar porphyrin macrocycles generated by peripheral steric crowding give the large red shifts but the structures internally constrained to be nonplanar do not; in the former case, the high order B_{1u} deformations are present, but in the latter they are significantly reduced (compare entries 1B and 3A/3B in Table 2).

Deformations in the out-of-plane modes change the torsion angles of the skeletal bonds and reduce the overlap of the π p-orbitals of the macrocycle atoms. This is true for all three B_{1u} modes as can be easily seen in Figure 2, but it is especially true for the $2B_{1u}$ and $3B_{1u}$ modes. For the latter two modes, the 2-Å deformations shown are about a factor of 10 over the size of deformations that are actually observed but serve to illustrate that these particular deformations cause large torsion angle changes, especially about the $C_\alpha-C_m$ bonds, thereby strongly reducing the p-orbital overlap in the $C_\alpha-C_m$ bonds and the π-conjugation in the ring. In fact, we find that the $2B_{1u}$ and $3B_{1u}$ deformations cause a disproportionately larger increase in the $N-C_\alpha-C_m-C_\alpha$ torsion angle when compared to the effect of the $1B_{1u}$ deformation. In other words, although the magnitudes of the $2B_{1u}$ and $3B_{1u}$ deformations are small, it is certainly conceivable that they could produce the observed large red shift. In this regard, it is also worth re-emphasizing how much smaller the high-order B_{1u} deformations are for the over-ruffled constrained NiT(Me)P structures (entries 3A, 3B in Table 2) compared to the optimized NiT(*t*Bu)P structure (entries 1A).

One way to evaluate the importance of the $2B_{1u}$ and $3B_{1u}$ contributions would be to reverse the NSD procedure; that is, we could add deformations together to generate structures that are composed of specified amounts of these out-of-plane deformations. Such an approach is problematical because, as originally pointed out by Hoard,[47,48] out-of-plane deformations

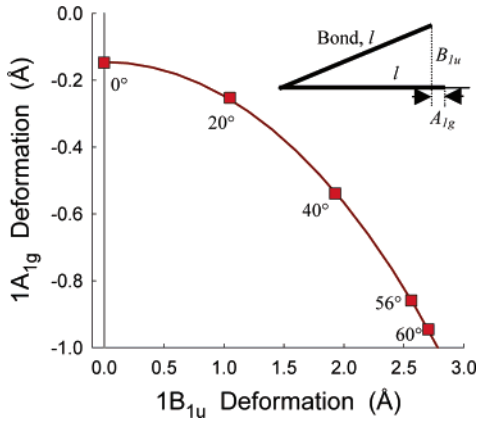

Figure 6. Illustration of the geometric relationship between $1B_{1u}$ out-of-plane and $1A_{1g}$ in-plane deformations of the porphyrin macrocycle using the structures of nickel tetramethylporphyrin constrained to various ruffling angles (0°, 20°, 40°, 56°, 60°) as calculated by molecular mechanics. The expression used to fit the data relates the contraction of the projection of a rigid bond into the mean plane of the porphyrin to the out-of-plane displacement of an atom of the bond. The expression obtained from simple trigonometric relationships is $A_{1g} = A_0 - l + \sqrt{l^2 - B_{1u}^2}$, where l is a fitting parameter interpreted as an effective radial bond length for the macrocycle and A_0 is the metal-induced contraction of the planar porphyrin relative to a reference Cu(II) porphine. The values of the fitting parameters l and A_0 for the nickel porphyrin curve shown are 4.957 Å and −0.145 Å (the small Ni(II) ion induces a small core contraction even when the porphyrin is planar).

and especially ruffling are associated with corresponding in-plane deformations due to radial contraction of the porphyrin core. This is a necessary consequence of the virtual invariability of the bond lengths compared to bond angles and torsion angles. For the calculated constrained NiT(Me)P structures, the relationship between the in-plane contraction (along the lowest-frequency $1A_{1g}$ deformation) and out-of-plane ruffling ($1B_{1u}$ deformation) is illustrated in Figure 6. The excellent least-squares fit to the theoretical expression (see caption of Figure 6) shows that the in-plane contraction is simply a geometrical consequence of the ruffling, in agreement with Hoard's conception. The in-plane deformations obtained from NSD should not be confused with IPNR.[49] Because of this coupling of in-plane and out-of-plane NSD deformations, the generation of physically meaningful structures using reverse NSD is not generally practicable, although it can be used to study the geometric consequences of the $2B_{1u}$ and $3B_{1u}$ deformations (see below).

Rather than try to generate structures from specified normal coordinate displacements, a more meaningful approach is to generate nonplanar porphyrins using various physical mechanisms different from peripheral steric crowding to see whether these structures also contain the $2B_{1u}$ and $3B_{1u}$ deformations missing in the internally constrained structures. We can then determine whether these structures produce large red shifts in

(47) Hoard, J. L. *N. Y. Acad. Sci.* **1973**, *206*, 18.
(48) Hoard, J. L. In *Porphyrins and Metalloporphyrins*; Smith, K. M., Ed.; Elsevier: Amsterdam, 1975; p 317.

(49) Most of the in-plane deformation found in the NSD analysis (Tables S8 and S9) trivially results from the out-of-plane deformations, as illustrated in Figure 6. For a nonplanar porphyrin, the projections of the atomic positions into the ring mean plane, when expressed by NSD in terms of the equivalent in-plane vibrational mode displacements, can appear to be significant even though the porphyrin bonds and angles do not change much. In fact, the NSD in-plane deformations would occur even if there were no changes in bond length and only the bond angle changes necessary to accommodate the out-of-plane distortion. In contrast, IPNR represents structural changes due to a direct substituent effect. In the NSD analysis, IPNR appears as additional small normal mode displacements caused by substituent-induced internal strain; the IPNR displacements will appear along only in-plane modes for planar porphyrins but along both the in-plane and out-of-plane modes for nonplanar porphyrins.

the UV−visible bands similar to those seen for the sterically crowded porphyrins. For calculation 6A in Tables 1 and 2, the macrocycle is forced to ruffle by introducing external van der Waals interactions with four extra atoms fixed in the mean plane near the *meso*-methyl groups. These fixed atoms are then removed and single-point INDO/S calculations carried out. For this protocol, the IPNR due to localized substituent−macrocycle interactions is absent, and this ruffling mechanism may better mimic the steric interactions that cause out-of-plane distortions of tetrapyrroles in proteins. For example, some hemoproteins contain hemes with moderately nonplanar structures that are thought to result primarily from nonbonding interactions with the surrounding protein (e.g., nitrophorins).[50] The energy-minimized NiT(Me)P structure obtained through external steric repulsion has approximately the same $3B_{1u}$ deformation as the energy-minimized structure of NiT(*t*Bu)P, but it has much less of the $2B_{1u}$ deformation (Table 2). As expected based on these high-order deformations, the INDO calculation does give a very large Soret red shift (1940 cm^{-1}) for this structure relative to the energy-minimized NiT(Me)P structure. Note that a part of this red shift may result from the position of the methyl group relative to the macrocycle, since a sizable value (6.4°) is found for δ (see Figure 5).

For another physically reasonable model structure, short hydrocarbon chains were attached across the opposing meso positions of NiT(Me)P to force the macrocycle to ruffle. When the chain contained eight methylene groups (compound **19**, entry 6B), the energy-minimized structure had approximately the same amount of $1B_{1u}$ deformation, a little less $2B_{1u}$ deformation, and slightly more $3B_{1u}$ deformation when compared with energy-minimized NiT(*t*Bu)P (Table 2). Again, the INDO calculation gives a large red shift (2684 cm^{-1} relative to energy-minimized NiT(Me)P). Approximately 5 nm of this 29-nm red shift (compared to entry 5) may result from the 4.8° movement of the *meso*-methylene groups above the $C_\alpha-C_m-C_\alpha$ plane (Figure 5). Most of the rest can be attributed to the high-order deformations, illustrating the profound consequences of these deformations.

Finally, a detailed examination of the $2B_{1u}$ and $3B_{1u}$ deformations suggests a more direct way to include these deformations in a constrained structure. As noted earlier, the $2B_{1u}$ and $3B_{1u}$ modes cause disproportionately large changes in the $N-C_\alpha-C_m-C_\alpha$ torsion angles. Thus, taking the structure of NiT(Me)P constrained to 56° (by twisting opposite pyrrole rings) and constraining the $N-C_\alpha-C_m-C_\alpha$ torsion angle to the value found in energy-minimized NiT(*t*Bu)P yields a structure that incorporates much of the $2B_{1u}$ and $3B_{1u}$ deformations found in the energy-minimized NiT(*t*Bu)P structure. As expected, INDO calculations for this structure again give a very large red shift (1913 cm^{-1}) in the Soret band (entry 6C). Although this doubly constrained structure accounts for almost all of the red shift in the absorption bands, even in this case other factors need to be considered; it is necessary to correct for the droopy methyl effect before essentially all of the red shift can be accounted for in the calculations (entry 7). Even then, the exact mixture of $2B_{1u}$ and $3B_{1u}$ deformations does not exactly match that seen for energy-minimized NiT(*t*Bu)P (entry 2); instead, it is likely that increased $3B_{1u}$ deformation may compensate for the reduced $2B_{1u}$ deformation.

Curiously, the mixture of $2B_{1u}$ and $3B_{1u}$ deformations generated by the four different mechanisms to ruffle NiT(Me)P (bulky substituents, intermolecular steric interactions, short straps, and additional torsional constraints) is somewhat different in each case. Typically, the $2B_{1u}$ deformation is more variable than the $1B_{1u}$ and $3B_{1u}$ deformations (Table 2 and Figure S2). For example, the $2B_{1u}$ deformation for energy-minimized NiT(*t*Bu)P is larger than that for the other two physically meaningful cases considered (Table 2). An examination of the deformation modes in Figure 2 suggests an obvious reason—the $2B_{1u}$ deformation mode moves the *meso* carbons toward one side of the porphyrin plane and the pyrrole β-carbons toward the other side of the porphyrin plane, making this deformation a very effective way to minimize local interaction between the bulky *tert*-butyl substituent and the pyrrole β-carbons. In contrast, for the $1B_{1u}$ and $3B_{1u}$ deformations, the *meso* carbons and pyrrole β-carbons move toward the same side of the porphyrin plane, making it difficult to relieve this localized steric interaction. Of course, all three B_{1u} modes move the *meso* carbon atoms (and their substituent) out of the mean plane, making all three deformations geometrically conducive to relieving the strain induced by steric crowding, short straps, or external steric interactions at the *meso* positions. Only for very bulky substituents such as *tert*-butyl should a large $2B_{1u}$ deformation be necessary to relieve local substituent steric strain.

The question then arises as to whether we can derive a simple structural interpretation of the effect of the contributions from the high-order B_{1u} modes? To do this, the NSD program was used in reverse to generate a structure with the $2B_{1u}$ and $3B_{1u}$ deformations of NiT(*t*Bu)P and no other out-of-plane deformations. At first glance, this porphyrin structure appears to be almost planar because the high-order deformations are so small. However, as mentioned earlier, closer inspection reveals that the small high-order deformations actually cause significant torsional strain to be introduced into the structure. Specifically, the $N-C_\alpha-C_m-C_\alpha$ torsion angle is 18° in this structure, a major portion of the 31° torsion angle found in the energy-minimized NiT(*t*Bu)P structure.

This finding suggests that the increase in the $N-C_\alpha-C_m-C_\alpha$ torsion angle directly causes the Soret red shift. As noted earlier, a NiT(Me)P structure formed by constraining the pyrrole dihedral angle to 56° and the $N-C_\alpha-C_m-C_\alpha$ torsion angle to 31° did give the large Soret red shift. It appears that an effect of the $2B_{1u}$ and $3B_{1u}$ deformations is simply to increase this torsion angle, already made large by the $1B_{1u}$ ruffling. Further, because of the structural relationship between $1B_{1u}$ ruffling and the other high-order B_{1u} deformations, it is likely that a large amount of ruffling will almost always bring along with it proportional contributions from the high-order B_{1u} deformations and thus give a large red shift of the UV−visible bands.[51]

To test this idea further, a plot of the calculated Soret wavelengths for all of the NiT(Me)P and NiT(*t*Bu)P structures (constrained and unconstrained) versus the $N-C_\alpha-C_m-C_\alpha$ torsion angle was prepared and is shown in Figure 7. The experimental data are also shown for comparison. Concomitant

(50) Roberts, S. A.; Weichsel, A.; Qiu, Y.; Shelnutt, J. A.; Walker, F. A.; Montfort, W. R. *Biochemistry* **2001**, *41*, 11327.

(51) A possible reason that the INDO/S calculations overshoot the observed red shifts is that our MM structures overestimate the contributions from high-order B_{1u} modes (see Figure S2).

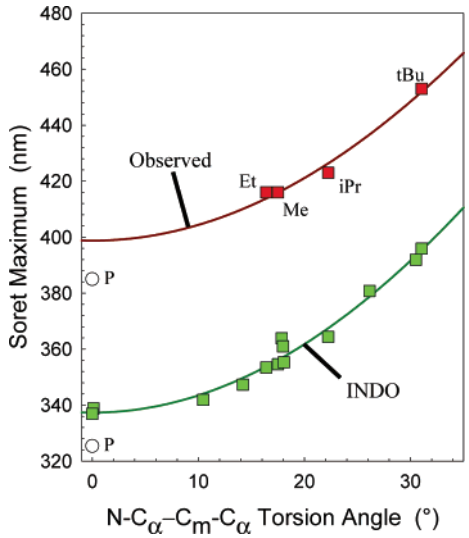

Figure 7. Soret band wavelengths from INDO/S calculations versus the $N-C_\alpha-C_m-C_\alpha$ torsion angles for all calculated NiT(Me)P and NiT(*t*Bu)P molecular mechanics structures, constrained and un-constrained. The porphine points are not included in the least-squares fits because of the electronic effect of the replacement of methyl groups with hydrogens. The curve is approximated by an equation of the form $\lambda = \lambda_0 + a(1 - \cos\theta)$ in which λ_0 and a are varied to obtain the fit. For the calculated data, λ_0 and a are 337.3 and 404.9 nm, respectively. The experimental points for the nickel tetraalkylporphyrins are included for comparison; the fit parameters are 398.7 and 370.7 nm for λ_0 and a, respectively.

with the increase in the torsion angle should be a decrease in the π p-orbital overlap, which is known to display a cosine dependence.[52] The dependence on the torsion angle displayed in Figure 7 is well approximated by a cosine function, suggesting that the disruption of the π bonding gives the resulting red shifts. The destabilization of the porphyrin $a_{2u}(\pi)$ orbital is the greatest, closing the gap between the HOMO's and LUMO's.[53] A similar dependence of the frequencies of the Raman structure-sensitive lines on the $N-C_\alpha-C_m-C_\alpha$ torsion angle was noted previously for the nickel tetraalkylporphyrin series.[5,54]

Discussion of Recent Studies Contradicting the Nonplanarity/Red-Shift Mechanism. The recent studies by Ghosh and DiMagno, while reaching the wrong conclusions, nevertheless have ultimately led to a more complete understanding of the various contributions to the band shifts. It is clear from the foregoing discussion that delineating electronic and structural effects on the optical spectra of nonplanar porphyrins can be complicated even for the tetraalkylporphyrins which have well-controlled conformational and electronic properties. It is important not only to choose appropriate model systems but also to be aware of possible systematic errors and artifacts in the calculations. For example, our findings indicate that the failure to reproduce the large red shifts in structures generated by using torsional constraints across the macrocycle, as reported here and elsewhere,[15] is in reality an artifact of the procedure used to constrain the macrocycle. Ruffling the porphyrin macrocycle in this manner simply does not generate the high-order $2B_{1u}$ and $3B_{1u}$ deformations that are a natural consequence of a strained porphyrin system. This artifact of the constraint method has led to an underestimation of the importance of nonplanarity and a mistaken belief that the missing Soret red shift is the result of IPNR.[15] Other methods of inducing the ruffling such as constraining the *z*-displacements of the *meso* carbons[16] to their values in energy-minimized NiT(*t*Bu)P give slightly more of the high-order B_{1u} deformations (see Table S19) and correspondingly larger red shifts (λ_{max} at 371.0 and 701.8 nm for the Soret and Q-bands, respectively) but still considerably underestimate the red shifts.

It is likely that some of the confusion surrounding the origin of the red shift is related to the nonlinear relationship between the Soret band red shift and ruffling (Figure 4). Because the nonplanarity-induced red shift may be small (as is the energy cost for this amount of deformation) when the change in nonplanarity occurs in the flat region below about 1.5 Å of ruffling, model compounds which differ in macrocyclic distortion within this region give such small band shifts that it is easy to lose the effect of nonplanarity within the variations due to substituent effects and other influences on the spectra. For example, simply replacing the four meso hydrogen atoms with methyl groups consistently causes a 15−20-nm red shift (Table S10), irrespective of the degree of ruffling or the metal in the core. This effect is far larger than the red-shift expected for a slight or moderate change in ruffling of the porphyrin in the flat region of the curve in Figure 4. A specific example from the literature[13,15] might be the strong electronic effects of the heptafluoropropyl substituents in the case of the tetrakis-(heptafluoropropyl)porphyrin model compounds used in some experimental studies that argued against the nonplanarity red-shift mechanism.[55]

Ruffling-Induced Red Shifts in the Soret Bands of Bridled Chiroporphyrins. The effect of nonplanar deformation on the optical properties of the porphyrin macrocycle was also investigated experimentally by using the series of bridled chiroporphyrins **12a**−**g**. In these compounds, the amount and type of deformation is expected to depend on the metal in the porphyrin core and the length of the straps connecting the adjacent meso positions. ^{1}H NMR spectroscopy was initially

(52) Streitwieser, J. A. *Molecular orbital theory for organic chemists*; Wiley: London, 1961.

(53) The shifts in the absorption bands ultimately arise from the frontier orbital energies and their destabilization upon twisting of the $C_\alpha-C_m$ bond. Examination of the orbital coefficients in the INDO results for NiP indicates that the a_{2u} HOMO has the most bonding character with respect to this bond. As the bond is twisted, the a_{2u} orbital is more destabilized than either the a_{1u} or e_g orbitals, thus narrowing the average gap between the HOMO's and LUMO's that mix to give the observed Soret and Q transitions and the observed red shift. For the lower symmetry of a ruffled porphyrin, the a_{1u} and e_g orbitals have more bonding character with respect to the $C_\alpha-C_m$ bond and are destabilized as the torsion angle increases but not to the extent of the a_{2u} orbital. Thus, the gap still decreases and a red shift still results. The bonding character of the a_{1u} and e_g orbitals probably results from orbital mixing.

(54) It is not currently known whether the molecular orbital shifts that give the absorption band shifts are purely a consequence of p_π orbital overlaps or if they involve the σ-electron system as well.

(55) The very nonplanar structure of $CoT(C_3F_7)P$ (d_{total} = 2.9 Å), which apparently does not show a red shift, highlights several of these potential problems.[13] In addition to a strong substituent electronic effect, we notice that the crystal structure of $CoT(C_3F_7)P$ is clearly anomalous compared to the related structures listed in Table S12 of the Supporting Information, and this structure may be unrepresentative of the true distortion of this porphyrin in solution. Supporting this idea, we notice that the corresponding free-base porphyrin structure published by DiMagno[76] a year prior to the Co(II) complex shows a nonplanar deformation of only about 1.3 Å, which is not much greater than that seen for other sterically un-crowded porphyrins (≤1.2 Å). In addition, the $CoT(C_3F_7)P$ structure does not fit with the expected trend of increased deformation for small metal ions, which is otherwise seen in Table S12 and also has been noted for other porphyrin complexes. In particular, MOETPP complexes show a large saddle distortion irrespective of the core metal and this saddle deformation increases for the smaller metals.[21] These considerations suggest that $T(C_3F_7)P$ is not intrinsically a very nonplanar porphyrin, is conformationally flexible as suggested by the calculations of Wondimagegn and Ghosh,[77] and is subject to crystal forces resulting in a structure for $CoT(C_3F_7)P$ that may not exist in other environments such as in solution.

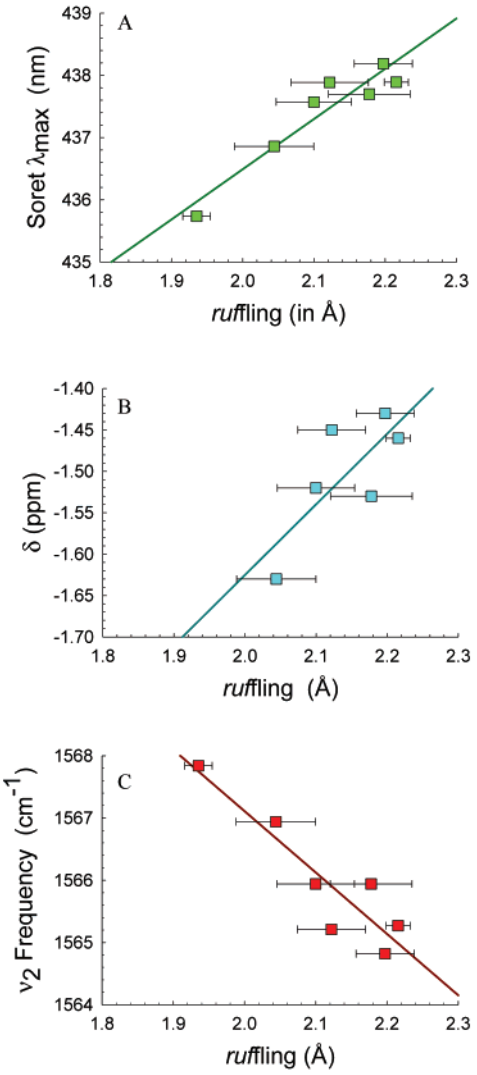

Figure 8. (A) Soret band peak wavelength versus ruffling deformation for **12a**−**g** (M = Ni); (B) ^{1}H NMR chemical shifts of the NH protons in **12b**−**g** (M = 2H) versus the ruffling deformation in **12b**−**g** (M = Ni); (C) Resonance Raman line frequencies versus the ruffling deformation for **12a**−**g** (M = Ni). Spectroscopic data for **12a**−**g** (M = Ni) (plots A and C) were measured in carbon disulfide, and data for **12a**−**g** (M = 2H) (plot B) was determined in deuteriochloroform.

used to determine the relative orientations of the meso substituents, i.e., whether the cyclopropyl groups were all on the same side of the macrocycle (αααα) or were alternately displaced toward opposite faces of the macrocycle (αβαβ).[56] Typically, the αβαβ conformation of the cyclopropyl substituents gives the lowest energy conformer, based on MM calculations for the unstrapped tetracyclopropylporphyrin analogue, with the αααα, αααβ, and ααββ conformers at significantly higher energy.[5] However, with a short eight-methylene strap attached (**12a**), the free-base porphyrin was found to adopt an αααα conformation of C_2 symmetry as shown by the two AB systems for the pyrrole protons in its ^{1}H NMR spectrum.[56] In contrast, the compounds with longer straps (**12b**−**g**) showed the expected αβαβ conformation of D_2 symmetry as evidenced by a pair of singlets for the β-pyrrolic protons.[56] This presumably reflects

(56) Gazeau, S.; Pécaut, J.; Marchon, J. C. *Chem. Commun.* **2001**, 1644.

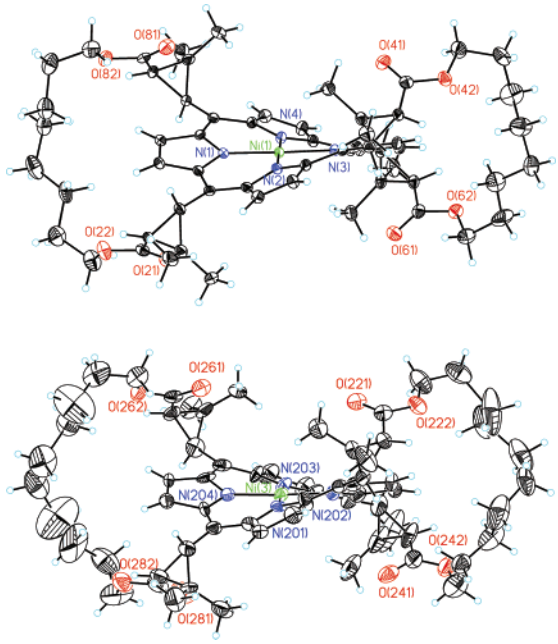

Figure 9. ORTEP views of selected molecules from the X-ray structures of crystals of the bridled chiroporphyrins: orthorhombic **12a** (M = Ni) (upper) and monoclinic **12c** (M = Ni).

the fact that with $n = 8$, the straps are too short to easily wrap around the porphyrin (Figure 9) thus destabilizing the αβαβ conformer. A similar switching of the conformation was seen for the corresponding zinc complexes, with **12a** (M = Zn) adopting the αααα conformation and **12b**−**g** (M = Zn) the αβαβ conformation. In contrast, all of the nickel complexes **12a**−**g** (M = Ni) showed αβαβ conformations by NMR, most likely because the small nickel atom strongly favors the ruffling of the porphyrin and thus the αβαβ conformer.

When plotted in Figure 8 versus the time-averaged ruffling of the nickel chiroporphyrin complexes obtained from MD simulations, the UV−visible, NMR, and Raman spectral parameters, which are all known to be affected by ruffling, show the expected correlations. Together, these findings provide further experimental evidence, if any was necessary, that the Soret red shifts arise from nonplanar distortion as suggested by many previous studies.[1,6,7] Specifically, the UV−visible spectra of the structurally homologous complexes **12a**−**g** (M = Ni) exhibit small Soret red shifts as the length of the chain increases. Only small red shifts are expected because the deformation changes over the whole series by only about 15%. The observed red shift increases to a maximum for a strap length of $n = 12$ and then declines slightly (Table S13); in fact, INDO/S calculations using energy-optimized structures of the chiroporphyrins reproduce this dependence on strap length. The red shift depends approximately linearly on the ruffling for the small range of ruffling values spanned by the series (Figure 8A).

That the red-shift indeed corresponds to ruffling of the porphyrin is supported by the fact that a similar dependence is observed with the two other spectroscopic measures of ruffling. As expected,[57] NMR shifts in the N−H protons of the free base chiroporphyrin series correlate with the ruffling deformation of the Ni complexes as shown in Figure 8B, although perhaps not as well as the UV−visible bands. The small downfield shift

(57) Pérollier, C.; Pécaut, J.; Ramasseul, R.; Marchon, J. C. *Inorg. Chem.* **1999**, *38*, 3758.

seen for the NH protons reflects a combination of a decrease in ring current[58] and an increase in intramolecular H-bonding.[26] The greater scatter could also result from plotting the free-base NMR resonances versus the Ni−porphyrin ruffling. Probably the most reliable indicators of macrocycle ruffling are the frequencies of the structure-sensitive marker lines (e.g., ν_2) in the high-frequency region (1340−1640 cm^{-1}) of the resonance Raman spectrum, which are known to shift to low frequency with increased ruffling.[5,34] For the chiroporphyrin series, the frequencies of these lines decrease with increasing strap length (Figure 8C), reaching a minimum when $n = 12$ (Table S13),[12] again indicating more ruffled structures for the longer straps. Thus, the shifts in the UV−visible, NMR, and resonance Raman spectra, all known indicators of nonplanar deformation,[1,6,7] consistently indicate that shorter chains inhibit out-of-plane distortion of the macrocycle. These trends are seen even though the structural changes are very small compared to the range of distortions investigated in other series of porphyrins.[1,6,7]

Summarizing, the moderate amount of ruffling distortion that results from the $\alpha\beta\alpha\beta$ conformation of the bulky *meso*-cyclopropyl groups is reduced if the chains are too short. This can be contrasted with most other strapped porphyrins for which shorter chains cause increased nonplanar deformation (e.g., entry 6B in Tables 1 and 2) and result in red-shifted absorption bands.[59−61] Thus regardless of the mechanism used to induce nonplanar distortion in strapped porphyrins, the more nonplanar porphyrins consistently give a red shift, and this red shift can usually be detected even when the change in deformation is small as it is for the bridled porphyrins.[62] Furthermore, compounds **12a**−**g** (M = Ni) provide a new way to determine whether red shifts are caused by the nonplanar deformation. For this chiroporphyrin series, the substituent effect is essentially identical in the series and, in addition, IPNR (if not negligible) might even be expected to change with strap length in the opposite direction for the chiroporphyrin series relative to other strapped porphyrin series.[63] Despite the latter consideration, the red shifts correlate with nonplanarity for all the known strapped porphyrins.

Crystal structures of **12a** (M = Ni) and **12c** (M = Ni) were obtained from two variants for each compound with orthorhombic or monoclinic crystal lattices. Each variant contained at least two independent molecules in the unit cell (Table S14 of the Supporting Information summarizes structural data for compounds **12a** (M = Ni) and **12c** (M = Ni) obtained from NSD analysis of all the X-ray structures). Details of the crystal structure of the monoclinic form of **12a** (M = Ni) have been reported in an earlier communication.[56] Figure 9 shows the crystal structure of one molecule of one crystalline form for **12a** (M = Ni) and **12c** (M = Ni). The crystal structures confirm the $\alpha\beta\alpha\beta$ stereochemistry of the substituents[3,56] and illustrate how the alkyl chains wrap around the edge of the porphyrin. A similar conformation is seen in all of the other crystalline forms of the nickel complexes.

The columns in Table S14 show the nonplanar deformations present in each of the lowest-energy out-of-plane normal modes of the porphyrin macrocycle, which typically encompass most of the nonplanar distortion. The nine structures of the bridled nickel chiroporphyrins show ruffling deformations of between 1.664 and 1.983 Å, with most of the nonplanar distortion being localized in the $1B_{1u}$ ruffling mode. For comparison, the MD-calculated average ruffling deformations for **12a** and **12c** (M=Ni) are 1.94 ± 0.02 and 2.10 ± 0.05 Å, respectively, only slightly higher than the range of total distortions observed in the crystal structures (Table S14). This in some measure validates our calculated structures and the use of MD to determine the deformations.

It is clear from the structural data that each independent molecule in the crystals exhibits a distinct degree of ruffling, with no apparent trend with the number of methylene groups. This suggests that packing forces are large enough to obscure the porphyrin conformational differences that exist in solution and prevent them from being detected in the X-ray data. Given the flexibility of the straps, it is not surprising that packing forces would be important for these porphyrins. The strap flexibility is the main reason for using the averaged deformations obtained from MD simulations, rather than energy-optimized MM structures, to determine the deformations. The MD procedure averages over many different conformations of the flexible straps, giving a better measure of the solution conformation than a single MM structure that might be trapped in a local minimum. We should also mention that the high-order B_{1u} modes also show about the expected time-average deformations. For example, the MD simulations give $2B_{1u}$ and $3B_{1u}$ deformations of 0.194 and 0.091 Å, respectively, for the chiroporphyrin with the 16-carbon straps (**12g**), while the corresponding average ruffling is 2.186 Å. These values are similar to those of the energy-optimized structure of NiT(*i*Pr)P at 2.203, 0.186, and 0.082 Å, respectively. Interestingly, there is also a trend toward larger $2B_{1u}$ deformations (0.229 Å for **12a**) as the straps shorten, signaling a stronger local steric interaction of the cyclopropyl group with the macrocycle (and possibly greater IPNR);[63] at the same time, the $3B_{1u}$ deformation remains nearly constant at 0.080 Å for **12a**.

Animations of the 0.1-ps snapshot structures show some interesting properties arising from the motion of the straps. A 200-ps animation for one of the bridled porphyrins is available at http://jasheln.unm.edu. From the animations, we notice that there are two possible orientations for the carbonyls of the ester groups of the bridles and that these two conformations interconvert on a nanosecond time scale. The carbonyl group can either be equatorially and inwardly pointing or can be axially and outwardly pointing. With four ester groups on the molecule there are six possible conformers based on the orientations of all of the carbonyl groups. During a 2-ns trajectory, several interconversions of individual carbonyl group are typically

(58) Medforth, C. J.; Muzzi, C. M.; Shea, K. M.; Smith, K. M.; Abraham, R. J.; Jia, S.; Shelnutt, J. A. *J. Chem. Soc., Perkin Trans. 2* **1997**, 839.
(59) Momenteau, M.; Mispelter, J.; Loock, B.; Bisagni, E. *J. Chem. Soc., Perkin Trans. 1* **1983**, 189.
(60) Simonis, U.; Walker, F. A.; Lee, P. L.; Hanquet, B. J.; Meyerhoff, D. J.; Scheidt, W. R. *J. Am. Chem. Soc.* **1987**, *109*, 2659.
(61) Ravikanth, M.; Chandrashekar, T. K. *J. Photochem. Photobiol.* **1993**, *74*, 181.
(62) Comparison of the UV−visible spectra of the zinc complexes **12a**,**b** (M = Zn) is also informative in this respect. The Soret band (434 nm) of the ruffled $\alpha\beta\alpha\beta$ complex **12b** (M = Zn) is indeed red shifted relative to the Soret band (429 nm) of the more planar $\alpha\alpha\alpha\alpha$ complex **12a** (M = Zn).[56]
(63) An important additional feature of the series of bridled porphyrins is that IPNR, if it is not negligible, should be largest for the short straps because they force the bulky substituents nearer to the mean plane and, consequently, to interact more strongly with the macrocycle atoms than for long straps, which relax these repulsive interactions by out-of-plane deformation. This stronger interaction with the macrocycle for the short straps must take place within a more planar macrocycle, leading to greater IPNR. Thus, if IPNR were important and caused a significant red shift, then we would expect the largest red shift for the short straps and the more planar porphyrin, contrary to the observed trend in the UV−visible data (Figure 8A and Table S13).

observed. In addition, there are also differences in the motion of the straps that depend on the strap length. The short straps are locked into the position shown in the X-ray structure with the strap bisecting the pyrrole β carbons at the crossing of the mean porphyrin plane. For the long straps, the straps move from side to side occupying three possible positions—the one that bisects the β carbons and two others located between the meso and β positions on either side of the pyrrole. The straps jump between these three plane-crossing positions, sometimes in concerted motions.

UV−Visible Band Red Shifts and Spectra−Structure Correlations. Some final general remarks should be made concerning the use of red shifts for structural correlations. Almost invariably, the spectral parameter observed in a structural correlation is not directly tied to the causal structural parameter but instead to a larger structural change that can be easily measured and that changes systematically with the causal parameter. An instructive example is the well-known negative correlation between some Raman line frequencies and the porphyrin core size.[64,65] In this case, it is thought that the actual cause of the frequency shift with core size is the small change in the $C_\alpha-C_m$ bond length, a Badger's rule type relationship, as the core-size marker lines are predominantly composed of stretching vibrations of this bond. However, the correlation (which holds for nearly planar porphyrins) is with the core size (center$-N_{pyrrole}$ distance), not the $C_\alpha-C_m$ bond length. The core size is simply a large structural change that can be accurately measured and which just happens to correlate with the $C_\alpha-C_m$ bond length and consequently the Raman frequency shifts.[66]

The indirect nature of most spectral correlations with structural parameters makes their application problematical. For example, one problem with using spectral correlations such as the Raman core-size correlation is that different types of distortion can give different correlations. In fact, the core-size correlation is only valid as long as the porphyrins being considered have about the same degree of nonplanarity. If not, then the nonplanar distortions twist the $C_\alpha-C_m$ bonds and also cause the $C_\alpha-N-C_\alpha$ bond angles to increase just as when the core size increases, e.g., due to metal substitution in near-planar porphyrins. In this way, the nonplanar distortion results in a change in the $C_\alpha-C_m$ bond lengths and a difference in the frequencies of the core-size marker lines. Because the nonplanar distortion changes systematically in a different way from the usual core-size correlation, a different relationship is observed.[5,41,67] In fact, because the core size contracts as the porphyrin ruffles, a positive correlation with core size is obtained for several series of nonplanar porphyrins[5,41,67] instead of the usual negative core-size correlation for the near planar porphyrins.[64,65,68]

Apparently, a similar situation exists for the correlation between the Soret red shift and ruffling of the porphyrin macrocycle. The structural parameter that we can easily measure is the deformation in the lowest-frequency $1B_{1u}$ mode (i.e., ruffling). However, it now appears that deformations along the two high-frequency B_{1u} modes also have a large influence on the red shift, and yet these deformations are typically so small that to measure them requires highly accurate crystal structures and NSD analysis. Therefore, just as in the case of the Raman core-size correlation, we must rely on a separate fortuitous relationship that may exist between the ruffling that we can measure ($1B_{1u}$) and the prevailing $2B_{1u}$ and $3B_{1u}$ deformations—relationships such as those illustrated in Figure S2. Both MM calculations and X-ray structures suggest that such relationships exist for physically meaningful distortion mechanisms, certainly for distortions caused by substituent crowding, strap-induced strain, and external steric perturbations that cause ruffling (Table 2), but apparently not for the internally constrained structures used in some recent studies.[15] There might also be physically significant cases for which relationships between the first-order and high-order modes do not exist, suggesting that the red-shift correlation with nonplanar distortion should be applied with great caution. Exercising caution in this regard in the use of the red shift/nonplanarity correlation is especially important because there are also other substituent-induced effects on the UV−visible spectra, including electron withdrawal/donation, hyperconjugation, and local substituent distortion such as vinyl rotation, which may make such correlations unreliable. The Raman structural correlations may have an advantage here in that the structure-sensitive lines are good markers of macrocyclic structure precisely because they are more or less insensitive to the nature of the substituents. On the other hand, the Raman nonplanarity correlation is known to be sensitive to other factors including IPNR in the form of the core-size correlation. Curiously, the Soret band shifts are apparently not very sensitive to IPNR, a distinct advantage if other factors affecting the red shifts are held constant or can be eliminated.

An important practical question is whether the ruffling/Soret-red-shift correlation might be usefully employed to obtain structural information about porphyrin cofactors in proteins. In our heme protein studies,[34,69−72] we have tended to avoid conclusions based only on heme absorption band shifts and have relied instead on the correlations with the frequencies of the Raman structure-sensitive marker lines.[5,8,23,28,64,65,67,73−75] Heme is especially problematical for spectra−structure correlations because of possible band shifts due to other spectral influences such as axial ligation, spin state, d-orbital configuration, and oxidation state, which are not of consequence for some other metal porphyrins, e.g., nickel porphyrins. Nevertheless, there is clearly a pressing need for spectral correlations with heme

(64) Spaulding, L. D.; Chang, C. C.; Yu, N.-T.; Felton, R. H. *J. Am. Chem. Soc.* **1975**, *97*, 2517.
(65) Spiro, T. G. In *Iron Porphyrins*; Lever, A. B. P., Gray, H. B., Eds.; Addison-Wesley: Reading, MA, 1982; Vol. Part II, p 89.
(66) In fact, the $C_\alpha-N-C_\alpha$ bond angle correlates with the frequencies of the core-size marker lines just as well as the core size and is more directly related to the $C_\alpha-C_m$ bond length through the α carbon. Nevertheless, even this correlation is somewhat indirect.
(67) Song, X.-Z.; Jentzen, W.; Jia, S.-L.; Jaquinod, L.; Nurco, D. J.; Medforth, C. J.; Smith, K. M.; Shelnutt, J. A. *J. Am. Chem. Soc.* **1996**, *118*, 12 975.
(68) For a series of metals in a nonplanar porphyrin, the slope of the core-size correlation depends on the intrinsic nonplanarity of the porphyrin ligand.[41]
(69) Ma, J. G.; Laberge, M.; Song, X. Z.; Jentzen, W.; Jia, S. L.; Zhang, J.; Vanderkooi, J. M.; Shelnutt, J. A. *Biochemistry* **1998**, *37*, 5118.
(70) Lu, Y.; Sousa, A.; Franco, R.; Mangravita, A.; Ferreira, G. C.; Moura, I.; Shelnutt, J. A. *Biochemistry* **2002**, *41*, 8253.
(71) Pauleta, S. R.; Lu, Y.; Goodhew, C. F.; Moura, I.; Pettigrew, G. W.; Shelnutt, J. A. *Biochemistry* **2001**, *40*, 6570.
(72) Ma, J. G.; Zhang, J.; Franco, R.; Jia, S.-L.; Moura, I.; Moura, J. J. G.; Kroneck, P. M. H.; Shelnutt, J. A. *Biochemistry* **1998**, *37*, 12431.
(73) Shelnutt, J. A.; Majumder, S. A.; Sparks, L. D.; Hobbs, J. D.; Medforth, C. J.; Senge, M. O.; Smith, K. M.; Miura, M.; Luo, L.; Quirke, J. M. E. *J. Raman Spectrosc.* **1992**, *23*, 523.
(74) Song, X.-Z.; Jaquinod, L.; Jentzen, W.; Nurco, D. J.; Jia, S.-L.; Khoury, R.; Ma, J.-G.; Medforth, C. J.; Smith, K. M.; Shelnutt, J. A. *Inorg. Chem.* **1998**, *37*, 2009.
(75) Li, X.-Y.; Czernuszewicz, R. S.; Kincaid, J. R.; Spiro, T. G. *J. Am. Chem. Soc.* **1989**, *111*, 7012.
(76) DiMagno, S. G.; Williams, R. A.; Therien, M. J. *J. Org. Chem.* **1994**, *59*, 6943.
(77) Wondimagegn, T.; Ghosh, A. *J. Phys. Chem. A* **2000**, *104*, 4606.

structure, and in cases where these other factors do not vary the red shift correlation might be useful. One drawback is that heme deformations in proteins are generally less than 1.5 Å, putting the changes in the flat region of the wavelength dependence (as illustrated in Figures 4 and 7) and thus band shifts due to structural changes will be small. On the positive side, substituent differences are absent in proteins, although for substituents such as the vinyl groups the rotational orientation also causes band shifts. In addition, in many cases the chromophore solvation environment within the protein is almost constant and might safely be neglected, e.g., in the case of structural differences resulting from protein conformational changes or site mutations. More complete studies of model nonplanar heme systems in known states could improve both Raman and UV−visible spectral correlations. Until these studies become available, the use of the UV−visible band red shifts as a measure of porphyrin nonplanarity in protein systems necessitates great caution and should be done in conjunction with other spectroscopic measures when possible. Even for isolated porphyrins or other tetrapyrroles, the red shift should be used as a diagnostic criterion for nonplanarity only after considering the dependence on substituent electronic and structural factors demonstrated by this and other studies.

Does ruffling cause large red shifts for highly nonplanar porphyrins? As we now see, the answer is ultimately somewhat complex, even for the tetraalkylporphyrins having conserved substituent patterns, similar substituent electronic effects, and a deformation of only one symmetry-type. If we mean ruffling in the loose sense often employed the answer is clearly yes. The summation of the B_{1u} nonplanar deformations does cause most of the large red-shift seen for MT(*t*Bu)P (M = Ni, Zn, or H_2) as suggested previously.[5] If we take the more precise definition of ruffling to mean only the deformation along the lowest-frequency $1B_{1u}$ mode, then technically the answer is no, as this deformation does not produce all of the observed red shift for the tetraalkylporphyrins. However, a pure $1B_{1u}$ deformation does produce an appreciable red shift, especially in the region of large ruffling. Perhaps the important point is that all three B_{1u} deformations are usually present and all three apparently cause red shifts of varying amounts in the tetraalkylporphyrins, and these will contribute with other factors to the observed shifts.

We have focused on the absorption band shifts in the present work, but most likely other chemical and biological properties will be influenced by these high-order mode deformations, which most certainly occur even for the moderate deformations appearing in proteins. Independent of the absorption band red-shift issue, we have demonstrated a combined NSD-MM-INDO computational framework that provides an effective methodology for quantifying macrocycle deformations and evaluating their effects on the electronic spectra of porphyrins, a technique that will prove applicable to the evaluation of other structural correlations.

Acknowledgment. We thank Nathalie Gon for help with the synthesis, Colette Lebrun for the mass spectra, and Dr. René Ramasseul for fruitful discussions. This work was partially supported by the Division of Materials Sciences and Engineering, Office of Basic Energy Sciences, U.S. Department of Energy. Sandia is a multiprogram laboratory operated by Sandia Corporation, a Lockheed-Martin company, for the United States Department of Energy under Contract DE-ACO4-94AL85000.

Supporting Information Available: Description of X-ray data analysis for the chiroporphyrins **12a** and **12c**; analytical data for compounds **12a**−**g** and **13a**−**g**; absorption maxima and structural data for sterically crowded and un-crowded free-base and nickel porphyrins; plots of the $2B_{1u}$ and $3B_{1u}$ deformations versus the $1B_{1u}$ deformation for MM structures and for X-ray structures; NSD results for X-ray and MM structures of T(C_3F_7)P and OETPP complexes; structural and spectroscopic data for bridled chiroporphyrins; full NSD results for selected crystal and MM structures; observed and calculated absorption maxima for nickel and zinc tetraalkylporphyrins and constrained ruffled structures; bond lengths and bond angles in NiT(Me)P and NiT(*t*Bu)P MM structures; NSD results of in-plane totally symmetric deformations for nickel and zinc tetraalkylporphyrin MM structures; X-ray crystallographic files (CIF) for the four structures of **12a** and **12c**. This material is available free of charge via the Internet at http://pubs.acs.org. Animations of a chiroporphyrin MD trajectory are viewable at http://jasheln.unm.edu using a web browser with the Chime plug-in. See any current masthead page for ordering information and Web access instructions.

JA0280933